Inflammation increases the penetrance of behavioral impairment in *Shank3* haploinsufficiency mice – can it explain the behavioral regression in Autism?

Authors: Sheng-Nan Qiao, PhD[1], Sung Eun Wang, PhD[1], Kun-Yong Kim, PhD[1], Sungsin Jo, PhD[5], Yong-Hui Jiang, MD, PhD [1-4]

Affiliation: [1]Department of Genetics, [2]Department of Neuroscience, [3]Department of Pediatrics, and [4]Department of Obstetrics, Gynecology & Reproductive Sciences, Yale University School of Medicine, New Haven, CT, USA

[5]Department of Biology, Soonchunhyang University, Soonchunhyang-ro 22, Sinchang-myeon, Asan, South Korea

Correspondence:

Yong-Hui Jiang, MD, PhD.

Department of Genetics, Neuroscience, Pediatrics, and OB/Gyn & Reproductive Sciences

TAC S317/S320

Yale University School of Medicine

300 Cedar St, New Haven, CT 06519

Tel: 203-785-2429

Email:yong-hui.jiang@yale.edu

Running title: Neuroinflammation Susceptibility in Autism

Abstract

Behavioral regression occurs in ~40% of *SHANK3*-associated autism spectrum disorder (ASD). We previously reported that significant behavioral regression in a small cohort with *SHANK3* haploinsufficiency patients, triggered by subclinical infections, responded to immunomodulator treatments. We hypothesize that behavioral regression results from the interplay between *SHANK3* deficiency and neuroinflammation. Using *Shank3* exon 4-22 deletion heterozygous mutant (*Sh3*$^{+/-}$) mouse, which shows no significant behavior impairments, we established a preclinical model – *Shank3* haploinsufficiency mouse undergoing systemic inflammation challenge via intraperitoneal injection of lipopolysaccharides (LPS). We found that, two weeks after LPS challenge, wild-type mice (WT) recovered but *Sh3*$^{+/-}$ mice exhibited motor impairment, anxiety-like behaviors, and excessive grooming, similar to *Shank3* exon 4-22 deletion homozygous mutants. Anti-inflammatory treatment partially reversed LPS-induced behavioral changes. Transcriptomic analysis revealed upregulation of neuroinflammation-related genes and downregulation of synaptic function-related genes in *Sh3*$^{+/-}$ mice in response to LPS. Especially, pro-inflammatory genes and microglia markers were overly activated that may result from the increased Toll-Like Receptor 4 (TLR4) expression in microglia in *Sh3*$^{+/-}$ mice. Our findings indicate that neuroinflammation increases the penetrance of behavioral impairment in *Shank3* haploinsufficiency mice and support a potential mechanism for the behavioral regression in human *SHANK3* disorders for future investigations.

Introduction

Autism spectrum disorder (ASD) is a group of neurodevelopmental conditions with typical onset before the age of three [1]. A significant proportion of children with ASD shows developmental arrest at an early developmental age and behavioral regression throughout the lifespan. Behavioral regression is characterized by loss of previously acquired skills, including loss of purposeful hand use, loss of acquired speech, and gait abnormalities [2-4]. Catatonic features are frequently associated with behavioral regression observed in ASD [5,6]. However, the underlying mechanism for the early developmental arrest and behavioral regression remains poorly understood.

The *SHANK3* mutation is one of the most common monogenic defects associated with ASD in humans [7-10]. Genetic mutations in *SHANK3* gene can manifest as Phelan-McDermid Syndrome (PMS), characterized by a chromosomal deletion of 22q13.3 or single nucleotide variants, indels, exonic deletions within the *SHANK3* gene in individuals with primary ASD [11]. Patients with *SHANK3* haploinsufficiency also exhibit severe intellectual disability, motor deficits, and speech delays [12-14]. Developmental regression with catatonic features has been reported in ~40% of cases with *SHANK3* haploinsufficiency [15-20]. We previously described four patients with pathogenic *SHANK3* mutations who experienced acute and severe behavioral regression following possible subclinical viral infections [21]. Notably, treatment with intravenous immunoglobulins (IVIG) combined with anti-inflammatory drugs and immunomodulators significantly reversed the behavioral regression in these cases [21]. This clinical report strongly suggests a potential link between inflammation and behavioral regression associated with *SHANK3*

63 haploinsufficiency. However, the direct causality could not be investigated and determined
64 from human studies.

65 SHANK3 protein is primarily characterized as a scaffold protein located at the
66 postsynaptic density of neurons, interacting with other synaptic proteins and affecting
67 synaptic function [22]. However, the role of SHANK3 in non-neuronal cells such as microglia
68 has been poorly studied [23-26]. Microglia activation is an important part of the innate
69 immune response in the brain and has been reported in ASD patients [27]. Our previous
70 studies showed that inflammation induces acute behavioral changes [28] and aggravates
71 hypothermia in *Shank3* mutant mouse model [29]. These initial findings suggest a potential
72 mechanistic link between *SHANK3* deficiency and inflammatory response.

73 Our lab previously generated a *Shank3* mutant mouse line with a deletion of exon
74 4 to 22 (*Shank3*$^{\Delta e4\text{-}22}$) that disrupts most of the *Shank3* coding region[30]. *Shank3*$^{\Delta e4\text{-}22}$
75 homozygous but not heterozygous mice showed robust face validity for autism-like
76 behaviors[30]. Therefore, *Shank3*$^{\Delta e4\text{-}22}$ heterozygous mice offer a unique opportunity to
77 examine the interaction between genes and environment, specifically whether
78 neuroinflammation may modify the penetrance of behavioral phenotypes associated with
79 *SHANK3* deficiency in humans. In this study, we utilized the *Shank3*$^{\Delta e4\text{-}22}$ heterozygous
80 mice and investigated the behavioral outcome, transcriptomic profiles, and microglia
81 activation after systemic inflammatory challenge induced by lipopolysaccharides (LPS).
82 These findings provide a general insight on the role of neuroinflammation in ASD
83 susceptibility.

Results

Systemic inflammation via LPS modified the penetrance of motor dysfunction, anxiety-like behavior, and repetitive behavior in *Shank3*$^{\Delta e4\text{-}22}$ heterozygous (*Sh3*$^{+/-}$) mice.

To explore whether inflammation plays a role in regression of ASD-associated behaviors, we challenged *Sh3*$^{+/-}$ mice by intraperitoneal injection of LPS (*Sh3*$^{+/-}$+ LPS). Control mice were given the same volume of normal saline (PBS) (*Sh3*$^{+/-}$ + PBS). Both LPS-treated *Sh3*$^{+/-}$ and wild-type (WT) mice experienced weight loss at 24 hours compared to PBS-treated mice (**Fig. 1A**). This indicated systemic inflammation induced by LPS, consistent with previous reports [31]. LPS-treated mice regained body weight at 72 hours post-injection, suggesting recovery from the LPS challenge (**Fig. 1A**). Acute behavioral changes, including decreased locomotor activity [32], social avoidance [33], and depressive-like behavior [34], have been reported in LPS-treated mice around 24 hours post-injection. However, interpretating these behavioral changes in the context of ASD model may be confounded by immediate sickness of test mice [28,35,36]. Therefore, we performed behavioral analysis two weeks after LPS injection to distinguish “LPS and SHANK3 haploinsufficiency interaction effect” vs. “acute LPS effect” (**Fig. 1B**). The *Shank3*$^{\Delta e4\text{-}22}$ homozygous (*Sh3*$^{-/-}$) group was included for a comparison [30].

To assess the motor coordination, latency to fall from the rotarod was measured in both steady speed (16 rpm) and accelerated speed (4-40 rpm) conditions. As expected, *Sh3*$^{-/-}$ mice showed significantly reduced latency to fall compared to WT+PBS group. No significant difference was observed between WT+PBS and WT+LPS groups, but *Sh3*$^{+/-}$ mice treated with LPS showed significantly shorter latency to fall than the PBS group (**Fig.**

107 **1C-D**). The duration of mouse spent in center of open field test (OFT) showed no
108 significant difference between WT+PBS and WT+LPS groups, but *Sh3*$^{+/-}$+LPS spent
109 significantly less time in the center compared to *Sh3*$^{+/-}$+PBS (**Fig. 1E**). In the light/dark
110 box test, distance of mouse moved in light chamber showed no significant difference
111 between WT+PBS and WT+LPS groups while *Sh3*$^{+/-}$+LPS significantly moved less in light
112 chamber compared to *Sh3*$^{+/-}$+PBS (**Fig. 1F**). Repetitive behavior was assayed through
113 scoring grooming behavior. *Sh3*$^{+/-}$+LPS showed significantly longer grooming duration
114 than *Sh3*$^{+/-}$+PBS while WT+PBS and WT+LPS groups were comparable (**Fig. 1G**). We
115 also conducted a three-chamber social preference test. As expected, *Sh3*$^{-/-}$ mice showed
116 no preference for social targets compared to WT. However, both LPS- and PBS-treated
117 *Sh3*$^{+/-}$ and WT mice spent significantly more time in the chamber with the social target (S)
118 or in the proximity region of the social target (SP) (**Fig. 1H-I**).

119 To explore potential sex effect, we compared motor function and sociability in both
120 PBS- and LPS-treated female and male *Sh3*$^{+/-}$ mice. LPS-treated male *Sh3*$^{+/-}$ mice
121 exhibited significant reduced latency to fall in rotarod, although no significant difference
122 found between LPS and PBS group in female *Sh3*$^{+/-}$ mice (**Supplementary Fig. 1A-B**).
123 Both LPS- and PBS-treated male *Sh3*$^{+/-}$ mice spent significantly more time in S or SP, but
124 no significant difference found in female *Sh3*$^{+/-}$mice (**Supplementary Fig. 1C-D**). Taken
125 together, our results indicated that, LPS treatment in *Sh3*$^{+/-}$ mice significantly impaired the
126 motor performance on rotarod, changed exploratory or anxiety-like behaviors in OFT and
127 light/dark box test, and increased grooming duration, but did not affect sociability in three-
128 chamber test. By comparison, LPS treatment in WT mice did not have any significant
129 effect on those behaviors. These findings suggest the interplay of inflammation and

130 *Shank3* haploinsufficiency in select domains of behaviors.

131 To assess whether anti-inflammation treatment can reverse the behavioral
132 changes induced by LPS in *Sh3*$^{+/-}$ mice, we applied mefenamic acid (MFA), a nonsteroidal
133 anti-inflammatory drug (NSAID). One of the MFA targets is the intracellular
134 cyclooxygenase (COX) signaling, which can be activated by LPS [37-39]. Previous study
135 also reported that MFA has neuroprotective effect [40]. Given that both WT+LPS and *Sh3*$^{+/-}$
136 +LPS group exhibited impaired motor function at 1 week after the LPS injection
137 (**Supplementary Fig. 2A-B**) but such behavior deficits of WT+LPS group recovered to
138 baseline at 2-week post-injection (**Fig. 1C-D**), we chose day 7 post-injection as the
139 endpoint of MFA treatment (**Fig. 2A**). We administered MFA via intraperitoneal injection
140 once a day for seven days following LPS injection and then performed rotarod test 24
141 hours after the final dose of MFA to evaluate the treatment efficacy (**Fig. 2A**). In the steady
142 speed (16 rpm) rotarod test, both WT+LPS+MFA and *Sh3*$^{+/-}$+LPS+MFA groups showed
143 significantly increased latency to fall compared to vehicle-treated groups (**Fig. 2B**),
144 suggesting that MFA effectively mitigated the motor function deficits induced by LPS.
145 *Sh3*$^{+/-}$+LPS+MFA showed trend of shorter latency to fall than WT+LPS+MFA (**Fig. 2B**, p
146 = 0.091), suggesting potential less pronounced anti-inflammatory efficacy and the
147 presence of exacerbated inflammatory responses in *Sh3*$^{+/-}$ mice. In contrast, in the
148 accelerated speed (4-40 rpm) rotarod test, MFA did not restore motor function in either
149 WT or *Sh3*$^{+/-}$ mice (**Fig. 2C**). Moreover, when comparing MFA treatment in female and
150 male *Sh3*$^{+/-}$ mice, MFA significantly increased latency to fall in female *Sh3*$^{+/-}$ mice but not
151 in male *Sh3*$^{+/-}$ mice (**Fig. 2D-E**). Overall, our results showed that LPS-induced motor
152 function impairment in *Sh3*$^{+/-}$ mice can be partially reversed by anti-inflammatory

153 treatment. Future studies will include additional behavioral assays, as well as time-course
154 and dose-dependent responses to MFA treatment.

155 **LPS-induced differentially expressed genes (DEGs) were associated with**
156 **neuroinflammation and neurotransmission in *Sh3*$^{+/-}$ mice.**

157 To understand how LPS-induced inflammation modifies the penetrance of motor
158 impairment in *Sh3*$^{+/-}$ mice, we analyzed the transcriptomic profiles in the forebrains by
159 bulk RNA-sequencing (RNA-seq) (**Supplementary Fig. 3A-B, Supplementary Tables 1**
160 **and 2**). LPS treatment induced hundreds of differentially expressed genes (DEGs) in both
161 WT and *Sh3*$^{+/-}$ mice compared to PBS-treated groups. The number of upregulated genes
162 (488 DEGs in *Sh3*$^{+/-}$+LPS vs. *Sh3*$^{+/-}$+PBS and 433 DEGs in WT+LPS vs. WT+PBS) was
163 greater than that of downregulated genes (75 DEGs in *Sh3*$^{+/-}$+LPS vs. *Sh3*$^{+/-}$+PBS and
164 108 DEGs in WT+LPS vs. WT+PBS) (**Fig. 3A-B**). We identified 88 upregulated and 37
165 downregulated DEGs between *Sh3*$^{+/-}$+LPS vs. WT+LPS (**Fig. 3C**). Although we found 67
166 upregulated and 33 downregulated genes when comparing transcriptomic profiles
167 between *Sh3*$^{+/-}$+PBS and WT+PBS (**Fig. 3D**), those genes barely overlapped with any
168 LPS-induced DEGs observed in *Sh3*$^{+/-}$ mice. Next, we compared the overlapping genes
169 among four comparisons (**Fig. 3E-F, Supplementary Tables 3 and 4**). A total of 313
170 shared upregulated and 12 shared downregulated DEGs were identified between
171 WT+LPS vs. WT+PBS and *Sh3*$^{+/-}$+LPS vs. *Sh3*$^{+/-}$+PBS. Those shared DEGs probably
172 represent the LPS-induced neuroinflammatory responses in mouse brains. Eight
173 upregulated genes shared among *Sh3*$^{+/-}$+LPS vs. WT+LPS, *Sh3*$^{+/-}$+LPS vs. *Sh3*$^{+/-}$+PBS
174 and WT+LPS vs. WT+PBS were well-known for their roles in neuroinflammation (**Fig. 3E**
175 highlighted with white underline, **Table 1**). Interestingly, 10 upregulated genes and 5

176 downregulated genes were found only in *Sh3*$^{+/-}$ mice not in WT mice in response to LPS
177 (**Fig. 3E-F** highlighted with green underline, **Table 2-3**), suggesting that LPS-induced
178 neuroinflammation in *Sh3*$^{+/-}$ mice is mediated by distinct signaling pathways. Additionally,
179 when we compared the overlapping genes between *Sh3*$^{+/-}$+PBS vs. WT+PBS and *Sh3*$^{+/-}$
180 +LPS vs. WT+LPS, only 4 genes in total (two are protein-coding genes) were identified
181 (**Fig. 3E-F** highlighted with red underline). Particularly, *Acr* is a *Shank3* subordinate
182 adjacent gene, whose expression increased when *Shank3* is deleted [41]. To further
183 characterize the function of DEGs from RNA-seq, we performed the pathway analysis
184 using the QIAGEN Ingenuity Pathway Analysis (IPA) [42]. We identified more activated
185 inflammation-associated pathways in response to LPS challenges in both *Sh3*$^{+/-}$ and WT
186 (**Supplementary Fig. 4 and 5**). In contrast, inhibited neurotransmission-related pathways
187 including NMDA receptor and calcium signaling pathways were only observed in LPS-
188 treated *Sh3*$^{+/-}$ but not in LPS-treated WT (**Supplementary Fig. 4 and 5**). To understand
189 the distinct molecular pathways in LPS-treated *Sh3*$^{+/-}$ mice, we delved into the pathway
190 analysis from *Sh3*$^{+/-}$+LPS vs. WT+LPS (**Supplementary Fig. 6**). The top five activated
191 pathways were all related to inflammatory processes. The top two inhibited pathways,
192 cardiac conduction and CREB signaling in neurons, represent inhibited neuron signal
193 transmission and neuronal functions. The other three inhibited pathways, HIF1α signaling,
194 eNOS signaling and phagosome formation pathways, represent increased neuronal
195 vulnerability to stress and inflammatory stimuli. In addition to the top five pathways with
196 highest z score value, we noticed that most of the upregulated signaling pathways in
197 response to LPS were all inflammation-related, including cytokine storm pathway and
198 neuroinflammation pathway (**Fig. 3G**). In contrast, the downregulated pathways in LPS-

199 treated *Sh3*$^{+/-}$ mice were neuronal and synaptic function-related, including potassium
200 channel pathway, glutamatergic signaling pathway, acetylcholine signaling pathway, and
201 gap junction signaling pathway (**Fig. 3G**). Overall, our RNA-seq results suggested that a
202 combination of exacerbated neuroinflammatory responses and impaired neuronal
203 functions is attributed to the LPS-induced behavioral regression in *Sh3*$^{+/-}$ mice.

204 **Neuroinflammation was increased in *Sh3*$^{+/-}$ mice**

205 To investigate how LPS leads to aggravated neuroinflammation in *Sh3*$^{+/-}$ brains,
206 we first measured the RNA expression of the pro-inflammatory cytokines *Il1b* and
207 chemokines *Cxcl10* using RT-qPCR. *Il1b* and *Cxcl10* have been identified as common
208 upregulated genes across all LPS-treated groups in RNA-seq (**Table 1**). RT-qPCR
209 confirmed that LPS significantly increased *Il1b* and *Cxcl10* expression in both WT and
210 *Sh3*$^{+/-}$ mice compared to PBS groups. Although no significant difference in *Il1b* and *Cxcl10*
211 expression was found between *Sh3*$^{+/-}$+PBS vs. WT+PBS, *Sh3*$^{+/-}$+LPS showed
212 significantly increased expression compared to WT+LPS group (**Fig. 4A-B**). A previous
213 study showed that LPS treatment upregulates microglia marker gene *Cx3cr1* while
214 downregulates microglia homeostasis gene *P2ry12* expression [43]. Therefore, we
215 examined the expression of microglia markers *Cx3cr1* and *P2ry12* using RT-qPCR. We
216 found that, as expected, LPS significantly increased *Cx3cr1* expression and decreased
217 *P2ry12* expression in both WT and *Sh3*$^{+/-}$ mice compared to PBS groups (**Fig. 4C-D**).
218 However, *Cx3cr1* expression was comparable between *Sh3*$^{+/-}$+PBS and WT+PBS but
219 significantly increased in *Sh3*$^{+/-}$+LPS compared to WT+LPS group (**Fig. 4C**). In contrast,
220 *P2ry12* expression was significantly higher in *Sh3*$^{+/-}$+PBS than in WT+PBS and higher in

221 *Sh3*$^{+/-}$+LPS than in WT+LPS (**Fig. 4D**).

222 We further examined microglia activation by examining the expression of IBA-1, a
223 marker widely used for the assessment of microglia activation state [44] (**Fig. 4E-H**).
224 Compared to PBS treatment, LPS increased IBA-1 staining significantly at 3 hours and
225 24 hours after LPS treatment in both WT and *Sh3*$^{+/-}$ mice. However, *Sh3*$^{+/-}$+LPS showed
226 significantly higher microglia activation than WT+LPS group at 24 hours but not at 3 hours
227 post-injection. These results indicated that the prolonged activation of microglia
228 contributed to increase of neuroinflammatory responses in *Sh3*$^{+/-}$ mice.

229 Next, to understand the mechanism underlying the LPS-induced microglia
230 overactivation, we analyzed the LPS transduction signaling pathways. LPS is known to
231 bind to Toll-like receptor-4 (TLR-4) [45], so we examined TLR4 expression using western
232 blot. We found that TLR4 expression was significantly higher in *Sh3*$^{+/-}$ than WT with either
233 PBS or LPS treatment (**Fig. 5A-B**). Additionally, we measured the SHANK3 protein
234 expression and found that either PBS- or LPS-treated *Sh3*$^{+/-}$ groups showed a reduction
235 in SHANK3 protein expression compared to WT groups as expected, but no changes in
236 SHANK3 expression were observed after LPS treatment (**Fig. 5C-D**).

237 TLR4 is known to associate with LPS-induced microglia activation[46-49]. To
238 investigate whether observed TLR4 augmentation directly facilitates microglia
239 overactivation in LPS treated *Sh3*$^{+/-}$ mice, we performed co-immunostaining of TLR4 and
240 microglia marker IBA1 and analyzed colocalization between TLR4 and IBA1 (**Fig. 5E-K**).
241 We found that TLR4 and IBA1 expression were well-colocalized in both LPS-treated WT
242 and *Sh3*$^{+/-}$ mice (**Fig. 5E-G**). However, colocalization coefficient normalized by TLR4 was
243 lower in *Sh3*$^{+/-}$ mice than that of WT mice. The colocalization coefficient normalized by

244 IBA1 was similar between *Sh3*$^{+/-}$ and WT mice (**Fig. 5H-I**), indicating elevated TLR4
245 expression in *Sh3*$^{+/-}$ might involve cell types in addition to microglia. Cellular
246 immunofluorescence intensity of IBA1 was significantly higher in *Sh3*$^{+/-}$ IBA1 than that of
247 WT (two-tailed p = 0.0001) (**Fig. 5K**), similar to prior results (**Fig. 4H**). In contrast, the
248 immunofluorescence intensity of TLR4 in *Sh3*$^{+/-}$ mice is slightly lower than WT (two-tailed
249 p = 0.0183) (**Fig. 5J**) and that is different from the results of immunoblot analysis using
250 fresh mouse brain tissue (**Fig. 5A-B**). Given that TLR4 was expressed in many different
251 cell types including astrocytes, neutrophils, and brain endothelial cells [50,51], these findings
252 supported that augmented TLR4 might also be in other cell types in addition to microglia
253 in *Sh3*$^{+/-}$ brains.

254 Finally, to validate whether behavior impairment is associated with synaptic
255 dysfunction in *Sh3*$^{+/-}$ mice, we analyzed the expression level of postsynaptic density (PSD)
256 protein HOMER 1b/c and PSD95, which play important roles in synaptic functions[52-54],
257 using forebrain PSD fraction at two-week post-injection of LPS (**Fig. 5L-N**). Consistent
258 with our prior report [30], HOMER 1b/c was significantly lower in *Sh3*$^{+/-}$ than WT but no
259 significant difference was found when comparing *Sh3*$^{+/-}$+LPS with *Sh3*$^{+/-}$+PBS group (**Fig.
260 5M**). In contrast, PSD95 was comparable between WT+PBS and *Sh3*$^{+/-}$+PBS groups but
261 significantly reduced in *Sh3*$^{+/-}$+LPS group compared to WT+LPS group. (**Fig. 5N**). These
262 results indicate that LPS treatment in SHANK3 haploinsufficiency mice causes a
263 significant but selective reduction of PSD95 protein that is known to be important for
264 synaptic functions and may contribute to the worsen behaviors in LPS treated Sh3$^{+/-}$ mice.

Table 1. Eight Upregulated DEGs shared among *Sh3*$^{+/-}$+LPS vs. WT+LPS, *Sh3*$^{+/-}$+LPS vs. *Sh3*$^{+/-}$+PBS and WT+LPS vs. WT+PBS.

Gene name	Protein function
Bcl3	BCL3 is an autonomous determinant of memory/terminal effector cell balance during CD8^{+} T cell differentiation in response to acute viral infection [55].
Ccl3	CCL3 as a cytokine contributes to progressive tissue damage and functional impairment during secondary injury after spinal cord injury [56].
Cxcl10	CXCL10 as a lymphocyte chemoattractant contributes to the intraparenchymal trafficking of lymphocytes during acute CNS inflammation [57].
Gbp5	GBP5 as a GTPase participates in the regulation of immunity and neuroinflammation [58].
Ifitm6	IFITM6 encodes cell surface proteins that modulate cell-cell adhesion and cell differentiation, is induced in various macrophages, and increases expression 24 hours after LPS [59].
Il1b	IL-1β can be acutely induced in the brain following peripheral bacterial infections, and microglia facilitate exaggerated IL-1β production upon exposure to acute systemic inflammation induced by bacterial LPS [60].
Steap4	STEAP4 as a key effector molecule contributes to the pathogenesis of neuroinflammation in experimental autoimmune encephalomyelitis [61].
Tlr2	Toll-like receptors (TLRs) are fundamental sensor molecules of the host innate immune system, which detect conserved molecular signatures of a wide range of microbial pathogens and initiate innate immune responses via distinct signaling pathways [62].

265

Table 2. Ten upregulated DEGs only shared between *Sh3*$^{+/-}$+LPS vs. WT+LPS and *Sh3*$^{+/-}$+LPS vs. *Sh3*$^{+/-}$+PBS, not include in WT+LPS vs. WT+PBS.

Gene name	Protein function
Alms1-ps1	ALMS1, centrosome and basal body associated, pseudogene 1.
Atf3	ATF3 as a transcription factor responds to and exert dual effects on inflammatory responses and in involved in neuroinflammatory response [63].
Ccl12	CCL12 as a chemokine expressed by microglia is involved in inflammation [64].
Fas	Fas/FasL pathway plays a key role in immune homeostasis and leads to excessive neuroinflammation during excessive neuroinflammation [65].
Gm11681	long non-coding RNA.
Hspa1a	HSPA1A and HSPA1B are two subtypes of HSPA1 proteins. HSPA1 is a member of the stress-inducible 70-kDa heat shock protein (HSP70) family, which plays a critical role in the cellular stress response [66,67].
Hspa1b	
Hspb1	
Oas1g	OAS1G is an important murine antiviral response factor, function through activating RNase L to degrade viral RNA in turn inhibiting viral replication and propagation [68].
Prok2	PROK2 is a secreted protein involved in the pathogenesis of several acute and chronic neurological diseases. It shows that PROK2 mediates neuronal cell deaths in traumatic brain injury via ferroptosis [69].

266

Table 3. Five downregulated DEGs only shared between *Sh3*$^{+/-}$+LPS vs. WT+LPS and *Sh3*$^{+/-}$+LPS vs. *Sh3*$^{+/-}$+PBS, not include in WT+LPS vs. WT+PBS.

Gene name	Protein function
4930415F15Rik	SPMIP7 protein is mainly involved in spermatogenesis but is also expressed in the brain and its function is unclear.
AC173482.5	Predicted gene, Gm47797
Gm14393	Predicted gene
Gm5111	Predicted gene
Tgif2	TGIF2 is a transcriptional repressor. Downregulation of TGIF2 is correlated with neuronal apoptosis and development of autism in mice [70].

267

268 **Discussion**

269 In this study, we successfully established a preclinical model and experimental
270 protocol to assess the role of neuroinflammation induced by LPS in *Sh3*$^{+/-}$ mice (**Fig. 6**).
271 We demonstrated that LPS challenge modified the penetrance of motor function deficits,
272 anxiety-like behavior, and repetitive behavior but did not alter social preference in *Sh3*$^{+/-}$
273 mice. More interestingly, the motor and emotion specific behavioral changes are
274 reminiscent of catatonia features that are often observed in humans with *SHANK3*
275 deficiency and idiopathic ASD [71-73]. Additionally, our extensive comparative transcriptome
276 analysis among the different groups validated the experimental protocol of LPS induction
277 and revealed distinct underlying molecular mechanisms. The significantly upregulated
278 genes ubiquitously associated with inflammatory pathways in LPS treated groups
279 indicated the effectiveness of LPS induction. The downregulated genes in multiple
280 pathways associated with neuronal and synaptic functions strongly support a potential
281 causal link between LPS treatment and increased penetrance of abnormal behaviors in
282 *Sh3*$^{+/-}$ mice. Moreover, the changes of the expression of microglia markers and increased
283 activation of microglia after LPS treatment are consistent with the role of
284 neuroinflammation in the brain. Finally, the partial reversal of motor impairment in LPS
285 treated *Sh3*$^{+/-}$ mice through the anti-inflammation treatment with MFA further supports this
286 causality. Notably, MFA treatment did not restore LPS-treated WT and *Sh3*$^{+/-}$ mice
287 performance in the accelerating speed rotarod. These findings suggest that the
288 mechanisms underlying inflammation-induced motor impairment are different between
289 steady speed and accelerating speed rotarod tests [74]. Additionally, one-week MFA
290 treatment was more effective in female *Sh3*$^{+/-}$ mice than male mice (**Fig. 2D-E**) and LPS-

291 treated male *Sh3*$^{+/-}$ mice performance was worse than female ones (**Supplementary Fig.**
292 **1A-B**), indicating potential sex difference in motor function[75] and neuroinflammation
293 process[76].

294 The behavior impairments induced by LPS in *Sh3*$^{+/-}$ mice could attribute to the
295 dysfunction of neuronal cells resulted from neuroinflammation. In the previous study that
296 our lab contributed, LPS challenge increased the excitability in D1 but not D2 medium
297 spiny neurons using whole-cell patch clamp recordings and decreased neuron calcium
298 transients in Nucleus Accumbens in response to social stimuli using *in vivo* Ca^{2+} imaging[28].
299 Our data showed that increased neuroinflammation downregulated genes associated
300 with neuronal and synaptic functions in *Sh3*$^{+/-}$ mice compared to WT mice and reduced
301 synaptic protein PSD95 in *Sh3*$^{+/-}$ mice.

302 LPS-induced neuroinflammation could also alter the function of non-neuronal cells
303 in *Sh3*$^{+/-}$ mice. Our findings of augmented TLR4 expression and microglia activation
304 associated with LPS treatment suggested that microglia are primarily involved in more
305 significant neuroinflammatory responses in *Sh3*$^{+/-}$ mice. Consistent with the findings in
306 many reports in literature supporting that TLR4 mediates microglial activation in brains [46-
307 49], our findings also support that the upregulation of TLR4 contributes to the observed
308 microglial activation following LPS administration. The direct causality between
309 upregulation of TLR4 and microglia activation due to LPS induction has been
310 demonstrated in a recent study[77]. Our observations are consistent with this finding and
311 support the augmented TLR4 as the cause of microglia activation in SHANK3 deficiency
312 mice. Further analysis of TLR4 and IBA1 cellular colocalization indicated that additional
313 cell types might also be involved in LPS-TLR4 (ligand-receptor) mediated

314 neuroinflammation. Our previous study showed that SHANK3 deficiency in periphery
315 nerve system contributes to the exaggerated inflammatory responses[78]. Our recently
316 published collaborative study has shown that conditional knock-out of SHANK3 major
317 isoform in brain endothelial cells recapitulated social behavior impairment and other
318 synaptic phenotypes [79]. Our findings are aligned with previous studies showing that
319 *Shank3* deficiency exacerbates the inflammatory responses in peripheral neurons either
320 induced by LPS [29,78] or by maternal immune activation during the pregnancy [80]. Overall,
321 our findings showed that LPS exacerbated neuroinflammation in *Sh3*$^{+/-}$ mouse brains
322 through unique molecular mechanisms as summarized in **Fig. 6** for further investigations
323 in future.

324 In humans, haploinsufficiency of *SHANK3* is highly penetrant for
325 neurodevelopmental impairments [81]. Approximately ~70% of PMS and *SHANK3*
326 deficiency patients met the diagnostic criteria for ASD. The comorbidity of intellectual
327 disability, anxiety, and epilepsy are highly penetrant or common [72]. There is an increasing
328 recognition of behavioral regression and catatonia among young teens with *SHANK3*
329 deficiency [71]. However, the triggers and mechanisms underlying the behavioral
330 regression are largely unknown. Although few clinical case reports implicated
331 neuroinflammation as a trigger [21,82], our findings may offer a mechanistic explanation for
332 the behavioral regressions observed in *SHANK3* patients after experiencing a subclinical
333 infection responded to the immune modulator treatment. Our study may support a link
334 between neuroinflammation and autism susceptibility in general.

335 Our results establish an important proof-of-concept study to dissect the link
336 between neuroinflammation and autism susceptibility. The apparent limitations of our

337 studies include that we have not provided definitive causality for the cell types and specific
338 molecular mechanism directly implicated in the increased neuroinflammatory responses
339 indued by LPS in SHANK3 haploinsufficiency mice. Future studies are warranted to
340 examine dosage- or treatment duration-dependent effects of LPS on behavioral outcomes
341 at different neurodevelopmental stages and in different sexes of *Shank3* deficiency mice.
342 Despite these limitations, our results suggest that *Shank3* haploinsufficiency increases
343 susceptibility to neuroinflammation-induced behavior impairment through distinct
344 molecular pathways. These findings provide new insights into the role of
345 neuroinflammation in ASD and for developing anti-inflammatory treatments as both
346 preventive and therapeutic strategies for behavior regression in ASD that are warranted
347 for further investigations.

348 **Materials and methods**

349 **Animals**

350 Animals were housed under standard 12 h/12 h light/dark cycles (7 AM-7 PM) with
351 food, water ad libitum, controlled temperature and humidity in the Yale University animal
352 facility. Experiments procedures conducted were following the Institutional Animal Care
353 and Use Committee (IACUC) protocol at Yale University (protocol No. 2025-20271).
354 *Shank3*$^{\Delta e4\text{-}22}$ mouse line (Jax Strain #:039524) was generated in-house and had been
355 crossed with C57BL/6J mouse line (Jax Strain #:000664) over 20 generations. Wild-type
356 (*WT*), *Shank3*$^{\Delta e4\text{-}22}$ homozygous (*Sh3*$^{-/-}$) and *Shank3*$^{\Delta e4\text{-}22}$ heterozygous mice (*Sh3*$^{+/-}$)
357 were obtained through heterozygotes breeding as previously described [30]. All experiment
358 procedures were performed within a time frame of 9 AM-5 PM. Animals of the same sex
359 were group housed (2-5 mice per cage). Both male and female mice were used. One
360 cage of mice with same genotype and same sex were assigned to PBS or LPS group
361 randomly. Experimental order of different group was randomized. Mice from multiple
362 groups for same experiments were carried out at same time. Before experiments, each
363 mouse was cataloged with identification number in an excel sheet which included detailed
364 information such as genotype and drug treatment. During experiments, experimenter
365 handled mice based on its identification number and attempted to be semi-blinded. Post-
366 processing, data handling and statistical analysis were semi-automated performed using
367 software stated below. Mice with health problems such as runt, fight wounds,
368 malocclusion, and eye problems, were excluded from experiments. For RNA and protein
369 extraction, mice were deeply anesthetized with 5% isoflurane, then mouse brains were
370 quickly collected, flash frozen in liquid nitrogen and stored in -80 °C freezer until further

371 use. The number of animals used in each experiment was determined based on our lab
372 prior experience and a prior power analysis was calculated using G*power statistics
373 software[83] (**Supplementary table 5**). Total number of mice used for each experiment was
374 as follows: 86 mice for MFA treatment rotarod test, 52-95 mice for open field, rotarod and
375 three-chamber behavior test, 49-66 mice for light/dark box and grooming behavior test,
376 15 mice for RNA sequencing, 40 mice for quantitative PCR, 24 mice for wide-field IBA1
377 staining, 6 mice for TLR4/IBA1 co-staining, 18 mice for whole-cell protein analysis and 24
378 mice for synaptic protein analysis. All experiments were replicated at least once, except
379 that RNA sequencing was done one time.

380 **Drug**

381 Three to five-week-old female and male mice were intraperitoneally injected with
382 LPS (Sigma, L6511) in saline at 1 mg/kg or same volume of saline (PBS). To test the
383 mefenamic acid (MFA) anti-inflammatory effect on behavior improvement, MFA
384 (Thermofisher, AAJ6270522) dissolved in DMSO at 5 mg/kg or the same volume of
385 DMSO (vehicle) was injected intraperitoneally to the mice with LPS injection once a day
386 for 7 days. Before injection, freshly made stock solution of MFA in DMSO (MFA treatment)
387 or DMSO (vehicle treatment) was diluted with 1:100 ratio in PBS to minimize DMSO
388 toxicity.

389 **Behavior assay**

390 For behavioral experiments, mice were handled for 3 days and habituated in the
391 procedure room for 1 hour before behavioral assays. All behavioral tests were conducted
392 once for each mouse.

393 Anxiety-like behaviors were tested by open field test (OFT) and light/dark box test
394 followed previous studies[30,84]. In OFT, mouse spontaneous activity in Noldus Open Field
395 (4 chambers, 40 (L) x 40 (W) x 30 (H) cm per chamber) over 10 minutes was recorded
396 with EthoVision XT video tracking software (Noldus). The Noldus two-chambered
397 light/dark box is equipped with the lid of dark chamber made by infrared translucent
398 material. The dimensions of the compartment are one third for the dark chamber (20 (L)
399 x 20 (W) x 20 (H) cm) and two thirds for the light chamber (20 (L) x 40 (W) x 20 (H) cm).
400 Mice were firstly placed into the open-light chamber (~700 lux) and given 5 min to freely
401 explore both light and dark (0 lux) chambers. The video was recorded with EthoVision XT
402 video tracking software. Ethovision software was used to automatically score the travel
403 distance and duration in arena.

404 Repetitive behavior was tested by evaluating mouse grooming behaviors. Mouse
405 was placed in a Noldus phenotyper (30 (L) x 30 (W) x 45 (H) cm) and recorded with
406 EthoVision XT video tracking software. Mouse freely explored for 10 minutes and last 5
407 minutes of grooming behavior was hand scored.

408 Motor coordination was tested by rotarod (Med Associate) performance as
409 described [30,85]. Mice were tested in two 5 min trials with an inter-trial interval of 30 min. In
410 accelerating session, revolutions per minute (rpm) of the turning barrel is accelerating
411 from 4 to 40. In steady speed session, the rpm of the turning barrel is fixed at 16. Latency
412 to fall, or to rotate off the top of the turning barrel, was measured by the timer.

413 Social preference was tested by a three-chamber assay as described[85]. An
414 unfamiliar age- and sex-matched mouse was used as a social stimuli mouse in the three-
415 chamber test and habituated under a wired enclosure for 3 days before testing. A

416 customized chamber composed of a rectangular Plexiglas arena (42 (L) x 56.5(W) x 35.8
417 (H) cm) divided into three chambers (each chamber 18.5 x 42 cm), with 2 doors
418 connecting chambers and two enclosures (wired pencil cups with metal vertical bars)
419 located in the two outer chambers. Briefly, the test mouse was habituated in the center
420 chamber for 5 min. Then the social stimuli mouse was placed under one of the pencil
421 cups and 2 doors were lifted allowing the experimental mouse to freely explore the whole
422 arena. The location of the empty and mouse enclosures, and the social stimuli mouse
423 were changed and counterbalanced for each trial. The EthoVision XT video tracking
424 software was used to score the duration of mouse spending in the empty chamber, the
425 mouse chamber, proximity regions (5 cm in distance) close to the empty enclosure, and
426 proximity regions close to the mouse enclosure.

427 **Bulk RNA sequencing**

428 Total RNA was isolated from the forebrain hemisphere using Trizol (Invitrogen,
429 15596018) followed manufacturer protocol and then treated with DNase I (Invitrogen,
430 AM1907) to remove contaminating DNA. RNA samples were sent to Yale Center for
431 Genome Analysis (YCGA) for bulk RNA sequencing (RNA-seq). See details about
432 sequencing process in Supplementary Information. After obtaining the data, low quality
433 reads were trimmed, and adaptor contamination were removed using Trim Galore (v0.5.0).
434 Trimmed reads were mapped to the mouse reference genome (mm10) using HISAT2
435 (v2.1.0) [86]. Gene expression levels were quantified using StringTie (v1.3.3b) [87].
436 Differentially expressed genes were identified using DESeq2 (v 1.22.1) [88]. Unpaired *t*-test
437 *p* value was used for filtering DEGs with significant differences between the two groups.
438 Log_2fold cutoff threshold at 1 and $p < 0.05$ was used to filter DEGs from two groups

439 comparison (WT+LPS vs. WT+PBS, *Sh3*$^{+/-}$+LPS vs. *Sh3*$^{+/-}$+PBS, *Sh3*$^{+/}$+LPS vs.
440 WT+LPS and *Sh3*$^{+/-}$+PBS vs. WT+PBS) for genes comparison and analysis. *Pathway*
441 *analysis*: QIAGEN Ingenuity Pathway Analysis (IPA) library of canonical pathways was
442 used to identify the pathways most significant to the data set. Molecules from the dataset
443 meeting the criteria in which $\log_2$fold cutoff threshold at 0.25 and $p < 0.05$ were associated
444 with a canonical pathway in the QIAGEN Knowledge Base were considered for the
445 analysis. Because using $\log_2$fold cutoff threshold at 1 only revealed three activated
446 pathways in *Sh3*$^{+/}$+LPS vs. WT+LPS comparison which were all inflammation-related, so
447 we expanded the $\log_2$fold cutoff threshold to 0.25. The significance of the association
448 between the data set and the canonical pathway was measured based on: 1) a ratio of
449 the number of molecules from the data set that map to the pathway divided by the total
450 number of molecules that map to the canonical pathway was displayed, 2) a right-tailed
451 Fisher's Exact Test was used to calculate a p-value determining the probability that the
452 association between the genes in the dataset and the canonical pathway was explained
453 by chance alone, 3) A z-score was calculated to indicate the likelihood of activation
454 or inhibition of that pathway. In this paper, pathways with right-tailed Fisher's Exact Test
455 $p < 0.05$, z-score > 0.1 was considered as activated pathways and z-score < -0.1 was
456 considered as inhibited pathways. The volcano plot was created using VolcaNoseR [89].
457 Veen diagram was plotted using InteractiVenn [90].

458 **Real-Time Quantitative Reverse Transcription PCR (RT-qPCR)**

459 Total RNA was isolated using same protocol as RNA-seq. RNA was transcribed
460 into cDNA using iScript cDNA Synthesis Kit (Bio-Rad, 1708890) and qPCR was performed
461 in triplicate using iQ SYBR Green Supermix (Bio-Rad, 1708880). Gene expressions were

462 normalized to the expression of GAPDH. Primers used to amplify cDNAs are: *Il1b,*
463 forward, TGGACCTTCCAGGATGAGGACA, reverse, GTTCATCTCGGAGCCTGTAGTG;
464 *Cxcl10,* forward, ATCATCCCTGCGAGCCTATCCT, reverse, GACCTTTTTTGGCTAAA
465 CGCTTTC; *Cx3cr1,* forward, GAGCATCACTGACATCTACCTCC, reverse, AGAAGGCA-
466 GTCGTGAGCTTGCA; *P2ry12* forward, CATTGACCGCTACCTGAAGACC, reverse,
467 GCCTCCTGTTGGTGAGAATCATG; *Gapdh* forward, CAAAATGGTGAAGGTCGGTG,
468 reverse, AATGAAGGGGTCGTTGATGG.

469 **Immunohistochemistry**

470 Transcardiac perfusion was conducted at both 3 hours and 24 hours after LPS or
471 PBS injection with 20 mL PBS then 20 mL 4% paraformaldehyde (PFA, Santa Cruz, sc-
472 281692). Mouse brains were collected, fixed in 4% PFA for 24 hours, then changed to 30%
473 (w/v) sucrose before sectioning. 50 μM brain sections between Bregma 1 mm to -1 mm
474 were obtained using vibratome (Leica, VT1200S). Primary antibody anti-Rabbit-IBA1
475 (1:200, FUJIFILM Wako Chemicals, 019-19741), anti-Mouse-TLR4 (1:100, Abcam,
476 ab22048), and secondary antibody Donkey Anti-Mouse Alexa Fluor® 488 (1:500, Abcam,
477 ab150105), Donkey anti-Rabbit Alexa Fluor™ 594 (1:500, Invitrogen, A-21207) were used.
478 Zeiss LSM 980 confocal microscopy with 20X objective len was used for wide-field IBA1
479 imaging. ImageJ was used for IBA1 fluorescence intensity quantification. Total 49 images
480 at 3 hours and 52 images at 24 hours were analyzed (**Fig. 4E-H**). Zeiss LSM 900 confocal
481 microscopy with 63X objective len was used for TLR4/IBA1 co-staining imaging and ZEN
482 Blue software was used for colocalization and fluorescence intensity analysis. Total 20
483 images were analyzed (**Fig. 5E-J**). Colocalization analysis was performed on a pixel-by-
484 pixel basis. Every pixel in the image was plotted in the scatter diagram based on its

485 intensity level from each channel. With setting the threshold in each channel, a scatter
486 plot with four quadrants was generated. Same threshold was used across all images and
487 pixels in colocalized quadrant were used for generating white "Colocalization mask"
488 images and further analysis. Software automatically measured colocalization coefficient
489 (Pearson's coefficient) and fluorescence intensity in each channel. Colocalization
490 coefficient normalized by TLR4 or IBA1 was calculated as sum of intensity of all pixels in
491 colocalized quadrant divided by sum of intensity of all pixels above the threshold value in
492 TLR4 channel or IBA1 channel ($\frac{\sum SumGreyCh_{1colocalized}}{\sum SumGreyCh_{1total}}$). Fluorescence intensity was
493 calculated as sum of all gray values from channel divided by the total number of pixels in
494 this channel ($\frac{\sum GreyCh1_i}{AreaCh1}$). Immunostaining and imaging were done under same condition
495 and same setting at same time across different groups. Biological triplicates of brain slices
496 from one mouse brain were employed. Results from at least three mice brains per group
497 were analyzed and compared.

498 **Western blot**

499 Western blot was performed as previously described [91]. Whole cell lysates from
500 mouse forebrain hemisphere were prepared using 1x lysis buffer (Cell Signaling
501 Technology, 9803S) containing 1x protease/phosphatase inhibitor (Cell Signaling
502 Technology, 5872S). Crude postsynaptic density (PSD) fraction from mouse forebrain
503 hemisphere were prepared following previously described protocol with some
504 modifications[30,92]. See details in Supplementary Information. Samples were boiled in 4x
505 Laemlli buffer (Bio-Rad, 161-0747) at 98 °C for 5 min before gel electrophoresis. Home-
506 made anti-rabbit SHANK3 C-terminus monoclonal antibody (1:1000), anti-rabbit TLR4

507 monoclonal antibody (1:1000, Santa Cruz, sc-293072), anti-mouse PSD95 monoclonal
508 antibody (1:1000, Invitrogen, MA1-046), HOMER 1b/c monoclonal HRP-conjugated
509 antibody (1:1000, Santa Cruz, sc-17842-HRP), and β-ACTIN monoclonal HRP-
510 conjugated antibody (1:1000, Invitrogen, MA5-15739-HRP) were used.

511 **Statistical analysis**

512 Graphpad Prism 10.0 (GraphPad Software) was used for the statistical analysis
513 and data plot. Differences were analyzed by student's *t*-test if comparing two variables or
514 using ANOVA if comparing more than two variables followed by multiple comparisons
515 either using statistical hypothesis testing with correction or planned comparisons without
516 correction. Significance was determined by two-tailed *t*-test *p* value or multiplicity adjusted
517 *p* value. For data which was not sampled from Gaussian distribution, a nonparametric
518 test was performed (**Fig. 4G-H**). Since unequal variance observed in LPS-evoked
519 cytokines and chemokines, Brown-Forsythe and Welch ANOVA tests were performed
520 (**Fig. 4A-B**). See detailed statistical analysis for each figure in **Supplementary Table 5**.
521 n represents the total number of data points per group, usually meaning the mice number
522 with an exception that n represents brain slice numbers (**Fig. 4G-H** and **Fig. 5G-K**). Both
523 sexes of mice were used and balanced across genotype and treatment, with an exception
524 that WT+PBS and WT+LPS groups were all male mice in RNA-seq experiments.
525 Behavioral difference between male and female mice were explored in **Supplementary**
526 **Fig. 1**. In **Fig. 1** and **Fig. 4,** individual data points were plotted as box plot: whiskers go
527 down to the smallest value and up to the largest value, box extends from the 25th to 75th
528 percentiles and line in the middle of the box is plotted at the median. In other figures,

529 individual data points were plotted and presented as average ± SEM. $p < 0.05$ was

530 considered statistically significant. BioRender was used to create schematic diagram.

531 **Authorship contribution statement**

532 S-N.Q. and Y-H.J. designed the experiments. S-N.Q. collected and analyzed the data.
533 S.W. manually scored grooming behavior. S.W., K-Y.K. and S.J. performed western blot.
534 S-N.Q. and Y-H.J. wrote and revised the manuscripts.

535 **Acknowledgement**

536 This work was supported by the National Institutes of Health (NIH) grant HD088007
537 MH104316, MH098114, MH117289, HD087795 (Y-H.J), the Autism Science Foundation
538 (ASF) fellowship (S-N.Q), and the National Research Foundation of Korea (NRF) grant
539 (RS-2024-00409006 to S.E.W and 2021R1A6A1-A03039503 to S.J). This work was
540 supported by the Rodent Behavior Analysis facility in Yale University funded by the Kavli
541 Institute of Neuroscience. The bulk RNA sequencing was supported by the National
542 Institute of General Medical Sciences of the National Institutes of Health under Award
543 Number 1S10OD030363-01A1.

544 **Conflict of Interest**

545 There are no competing financial interests in relation to the work described.

546 **Reference**

547 1 Regier, D. A., Kuhl, E. A. & Kupfer, D. J. The DSM-5: Classification and criteria changes.
548 *World Psychiatry* **12**, 92-98 (2013). https://doi.org/10.1002/wps.20050

549 2 Stefanatos, G. A. Regression in autistic spectrum disorders. *Neuropsychol Rev* **18**,
550 305-319 (2008). https://doi.org/10.1007/s11065-008-9073-y

551 3 Manelis, L. *et al.* Language regression is associated with faster early motor
552 development in children with autism spectrum disorder. *Autism Res* **13**, 145-156
553 (2020). https://doi.org/10.1002/aur.2197

554 4 Boterberg, S., Van Coster, R. & Roeyers, H. Characteristics, Early Development and
555 Outcome of Parent-Reported Regression in Autism Spectrum Disorder. *J Autism Dev*
556 *Disord* **49**, 4603-4625 (2019). https://doi.org/10.1007/s10803-019-04183-x

557 5 Kohlenberg, T. M. *et al.* Psychiatric illness and regression in individuals with Phelan-
558 McDermid syndrome. *J Neurodev Disord* **12**, 7 (2020).
559 https://doi.org/10.1186/s11689-020-9309-6

560 6 Ghaziuddin, M. Catatonia: A Common Cause of Late Regression in Autism. *Front*
561 *Psychiatry* **12**, 674009 (2021). https://doi.org/10.3389/fpsyt.2021.674009

562 7 Betancur, C. & Buxbaum, J. D. SHANK3 haploinsufficiency: a "common" but
563 underdiagnosed highly penetrant monogenic cause of autism spectrum disorders.
564 *Mol Autism* **4**, 17 (2013). https://doi.org/10.1186/2040-2392-4-17

565 8 Satterstrom, F. K. *et al.* Large-Scale Exome Sequencing Study Implicates Both
566 Developmental and Functional Changes in the Neurobiology of Autism. *Cell* **180**,
567 568-584 e523 (2020). https://doi.org/10.1016/j.cell.2019.12.036

568 9 Zhou, X. *et al*. Integrating de novo and inherited variants in 42,607 autism cases
569 identifies mutations in new moderate-risk genes. *Nat Genet* (2022).
570 https://doi.org/10.1038/s41588-022-01148-2
571 10 Fu, J. M. *et al*. Rare coding variation provides insight into the genetic architecture and
572 phenotypic context of autism. *Nat Genet* (2022). https://doi.org/10.1038/s41588-
573 022-01104-0
574 11 Nevado, J. *et al*. Variability in Phelan-McDermid Syndrome in a Cohort of 210
575 Individuals. *Front Genet* **13**, 652454 (2022).
576 https://doi.org/10.3389/fgene.2022.652454
577 12 Soorya, L. *et al*. Prospective investigation of autism and genotype-phenotype
578 correlations in 22q13 deletion syndrome and SHANK3 deficiency. *Mol Autism* **4**, 18
579 (2013). https://doi.org/10.1186/2040-2392-4-18
580 13 Leblond, C. S. *et al*. Meta-analysis of SHANK Mutations in Autism Spectrum Disorders:
581 a gradient of severity in cognitive impairments. *PLoS Genet* **10**, e1004580 (2014).
582 https://doi.org/10.1371/journal.pgen.1004580
583 14 Serrada-Tejeda, S., Martínez-Piédrola, R. M., Máximo-Bocanegra, N., Sánchez-
584 Herrera-Baeza, P. & Pérez-de-Heredia-Torres, M. Descriptive Analysis of Adaptive
585 Behavior in Phelan-McDermid Syndrome and Autism Spectrum Disorder. *Frontiers in*
586 *neuroscience* **16**, 893003 (2022). https://doi.org/10.3389/fnins.2022.893003
587 15 Reierson, G. *et al*. Characterizing regression in Phelan McDermid Syndrome (22q13
588 deletion syndrome). *J Psychiatr Res* **91**, 139-144 (2017).
589 https://doi.org/10.1016/j.jpsychires.2017.03.010

590 16 Denayer, A. *et al*. Neuropsychopathology in 7 Patients with the 22q13 Deletion
591 Syndrome: Presence of Bipolar Disorder and Progressive Loss of Skills. *Molecular*
592 *Syndromology* **3**, 14-20 (2012). https://doi.org/10.1159/000339119
593 17 Zwanenburg, R. J., Ruiter, S. A. J., van den Heuvel, E. R., Flapper, B. C. T. & Van
594 Ravenswaaij-Arts, C. M. A. Developmental phenotype in Phelan-McDermid (22q13.3
595 deletion) syndrome: a systematic and prospective study in 34 children. *Journal of*
596 *Neurodevelopmental Disorders* **8**, 16 (2016). https://doi.org/10.1186/s11689-016-
597 9150-0
598 18 Serret, S. *et al*. Lithium as a rescue therapy for regression and catatonia features in
599 two SHANK3 patients with autism spectrum disorder: case reports. *BMC Psychiatry*
600 **15**, 107 (2015). https://doi.org/10.1186/s12888-015-0490-1
601 19 Phelan, K. & McDermid, H. E. The 22q13.3 Deletion Syndrome (Phelan-McDermid
602 Syndrome). *Mol Syndromol* **2**, 186-201 (2012). https://doi.org/10.1159/000334260
603 20 Phelan, K. *et al*. Phelan-McDermid syndrome: a classification system after 30 years
604 of experience. *Orphanet J Rare Dis* **17**, 27 (2022). https://doi.org/10.1186/s13023-
605 022-02180-5
606 21 Bey, A. L. *et al*. Subacute Neuropsychiatric Syndrome in Girls With SHANK3 Mutations
607 Responds to Immunomodulation. *Pediatrics* **145**, e20191490 (2020).
608 https://doi.org/10.1542/peds.2019-1490
609 22 Durand, C. M. *et al*. Mutations in the gene encoding the synaptic scaffolding protein
610 SHANK3 are associated with autism spectrum disorders. *Nat Genet* **39**, 25-27 (2007).
611 https://doi.org/10.1038/ng1933

612 23 He, G. *et al*. Dexmedetomidine attenuates neuroinflammation and microglia
613 activation in LPS-stimulated BV2 microglia cells through targeting circ-Shank3/miR-
614 140-3p/TLR4 axis. *Eur J Histochem* **67** (2023). https://doi.org/10.4081/ejh.2023.3766
615 24 Fischer, I. *et al*. Hyperbaric Oxygen Therapy Alleviates Social Behavior Dysfunction
616 and Neuroinflammation in a Mouse Model for Autism Spectrum Disorders. *Int J Mol*
617 *Sci* **23** (2022). https://doi.org/10.3390/ijms231911077
618 25 Cope, E. C. *et al*. Immature Neurons and Radial Glia, But Not Astrocytes or Microglia,
619 Are Altered in Adult Cntnap2 and Shank3 Mice, Models of Autism. *eNeuro* **3** (2016).
620 https://doi.org/10.1523/eneuro.0196-16.2016
621 26 Urrutia-Ruiz, C. *et al*. Deletion of the Autism-Associated Protein SHANK3 Abolishes
622 Structural Synaptic Plasticity after Brain Trauma. *Int J Mol Sci* **23** (2022).
623 https://doi.org/10.3390/ijms23116081
624 27 Uchino, S. & Waga, C. Novel Therapeutic Approach for Autism Spectrum Disorder:
625 Focus on SHANK3. *Curr Neuropharmacol* **13**, 786-792 (2015).
626 https://doi.org/10.2174/1570159x13666151029105547
627 28 Tzanoulinou, S. *et al*. Inhibition of Trpv4 rescues circuit and social deficits unmasked
628 by acute inflammatory response in a Shank3 mouse model of Autism. *Molecular*
629 *Psychiatry* **27**, 2080-2094 (2022). https://doi.org/10.1038/s41380-021-01427-0
630 29 Zhang, L. *et al*. SHANK3 in vagal sensory neurons regulates body temperature,
631 systemic inflammation, and sepsis. *Front Immunol* **14**, 1124356 (2023).
632 https://doi.org/10.3389/fimmu.2023.1124356

633 30 Wang, X. *et al*. Altered mGluR5-Homer scaffolds and corticostriatal connectivity in a
634 Shank3 complete knockout model of autism. *Nat Commun* **7**, 11459 (2016).
635 https://doi.org/10.1038/ncomms11459
636 31 Piirsalu, M. *et al*. Treatment With Lipopolysaccharide Induces Distinct Changes in
637 Metabolite Profile and Body Weight in 129Sv and Bl6 Mouse Strains. *Frontiers in*
638 *Pharmacology* **11** (2020). https://doi.org/10.3389/fphar.2020.00371
639 32 Jung, H. *et al*. LPS induces microglial activation and GABAergic synaptic deficits in
640 the hippocampus accompanied by prolonged cognitive impairment. *Scientific*
641 *Reports* **13**, 6547 (2023). https://doi.org/10.1038/s41598-023-32798-9
642 33 Decker Ramirez, E. B. *et al*. The effects of lipopolysaccharide exposure on social
643 interaction, cytokine expression, and alcohol consumption in male and female mice.
644 *Physiology & Behavior* **265**, 114159 (2023).
645 https://doi.org/https://doi.org/10.1016/j.physbeh.2023.114159
646 34 O'Connor, J. C. *et al*. Lipopolysaccharide-induced depressive-like behavior is
647 mediated by indoleamine 2,3-dioxygenase activation in mice. *Mol Psychiatry* **14**, 511-
648 522 (2009). https://doi.org/10.1038/sj.mp.4002148
649 35 Parrott, J. M., Oster, T. & Lee, H. Y. Altered inflammatory response in FMRP-deficient
650 microglia. *iScience* **24**, 103293 (2021). https://doi.org/10.1016/j.isci.2021.103293
651 36 Hodges, S. L. *et al*. Lipopolysaccharide-induced inflammation leads to acute
652 elevations in pro-inflammatory cytokine expression in a mouse model of Fragile X
653 syndrome. *Physiol Behav* **215**, 112776 (2020).
654 https://doi.org/10.1016/j.physbeh.2019.112776

655 37 Eliopoulos, A. G., Dumitru, C. D., Wang, C. C., Cho, J. & Tsichlis, P. N. Induction of
656 COX-2 by LPS in macrophages is regulated by Tpl2-dependent CREB activation
657 signals. *Embo j* **21**, 4831-4840 (2002). https://doi.org/10.1093/emboj/cdf478
658 38 Blais, V., Turrin, N. P. & Rivest, S. Cyclooxygenase 2 (COX-2) inhibition increases the
659 inflammatory response in the brain during systemic immune stimuli. *J Neurochem* **95**,
660 1563-1574 (2005). https://doi.org/10.1111/j.1471-4159.2005.03480.x
661 39 Cimolai, N. The potential and promise of mefenamic acid. *Expert Review of Clinical*
662 *Pharmacology* **6**, 289-305 (2013). https://doi.org/10.1586/ecp.13.15
663 40 Khansari, P. S. & Halliwell, R. F. Evidence for neuroprotection by the fenamate NSAID,
664 mefenamic acid. *Neurochemistry International* **55**, 683-688 (2009).
665 https://doi.org/https://doi.org/10.1016/j.neuint.2009.06.014
666 41 Lu, X. *et al.* Transcriptional determinism and stochasticity contribute to the
667 complexity of autism-associated SHANK family genes. *Cell Rep* **43**, 114376 (2024).
668 https://doi.org/10.1016/j.celrep.2024.114376
669 42 Krämer, A., Green, J., Pollard, J., Jr. & Tugendreich, S. Causal analysis approaches in
670 Ingenuity Pathway Analysis. *Bioinformatics* **30**, 523-530 (2014).
671 https://doi.org/10.1093/bioinformatics/btt703
672 43 Sousa, C. *et al.* Single-cell transcriptomics reveals distinct inflammation-induced
673 microglia signatures. *EMBO Rep* **19** (2018).
674 https://doi.org/10.15252/embr.201846171
675 44 Norden, D. M., Trojanowski, P. J., Villanueva, E., Navarro, E. & Godbout, J. P.
676 Sequential activation of microglia and astrocyte cytokine expression precedes

677 increased Iba-1 or GFAP immunoreactivity following systemic immune challenge.
678 *Glia* **64**, 300-316 (2016). https://doi.org/10.1002/glia.22930
679 45 Tiwari, P. C. & Pal, R. The potential role of neuroinflammation and transcription
680 factors in Parkinson disease. *Dialogues Clin Neurosci* **19**, 71-80 (2017).
681 https://doi.org/10.31887/DCNS.2017.19.1/rpal
682 46 Cartarozzi, L. P., de Melo Lima, B. H., Tomiyama, A. L. R. M., Santos, F. R. & de Oliveira,
683 A. L. R. Toll-like receptors 2 and 4 influence neuronal survival and glial reactions
684 following ventral root crush injury in mice. *Journal of Neuroimmunology* **406**, 578655
685 (2025). https://doi.org/https://doi.org/10.1016/j.jneuroim.2025.578655
686 47 Yao, L. *et al*. Toll-like receptor 4 mediates microglial activation and production of
687 inflammatory mediators in neonatal rat brain following hypoxia: role of TLR4 in
688 hypoxic microglia. *Journal of Neuroinflammation* **10**, 785 (2013).
689 https://doi.org/10.1186/1742-2094-10-23
690 48 Jiang, Y. *et al*. Evobrutinib mitigates neuroinflammation after ischemic stroke by
691 targeting M1 microglial polarization via the TLR4/Myd88/NF-κB pathway. *Mol Med* **31**,
692 148 (2025). https://doi.org/10.1186/s10020-025-01203-8
693 49 Zhu, J. *et al*. Toll-like receptor 4 deficiency in Purkinje neurons drives cerebellar ataxia
694 by impairing the BK channel-mediated after-hyperpolarization and cytosolic calcium
695 homeostasis. *Cell Death Dis* **15**, 594 (2024). https://doi.org/10.1038/s41419-024-
696 06988-w
697 50 *TLR4 expression in the Human Protein Atlas*,
698 <https://www.proteinatlas.org/ENSG00000136869-TLR4/single+cell> (

699 51 Sjöstedt, E. *et al*. An atlas of the protein-coding genes in the human, pig, and mouse
700 brain. *Science* **367**, eaay5947 (2020). https://doi.org/10.1126/science.aay5947
701 52 Levy, A. M., Gomez-Puertas, P. & Tümer, Z. Neurodevelopmental Disorders
702 Associated with PSD-95 and Its Interaction Partners. *Int J Mol Sci* **23** (2022).
703 https://doi.org/10.3390/ijms23084390
704 53 Jung, S. & Park, M. Shank postsynaptic scaffolding proteins in autism spectrum
705 disorder: Mouse models and their dysfunctions in behaviors, synapses, and
706 molecules. *Pharmacol Res* **182**, 106340 (2022).
707 https://doi.org/10.1016/j.phrs.2022.106340
708 54 Shiraishi-Yamaguchi, Y. & Furuichi, T. The Homer family proteins. *Genome Biology* **8**,
709 206 (2007). https://doi.org/10.1186/gb-2007-8-2-206
710 55 Jaiswal, H. *et al*. The NF-κB regulator Bcl-3 restricts terminal differentiation and
711 promotes memory cell formation of CD8+ T cells during viral infection. *PLoS Pathog*
712 **17**, e1009249 (2021). https://doi.org/10.1371/journal.ppat.1009249
713 56 Pelisch, N., Rosas Almanza, J., Stehlik, K. E., Aperi, B. V. & Kroner, A. CCL3 contributes
714 to secondary damage after spinal cord injury. *J Neuroinflammation* **17**, 362 (2020).
715 https://doi.org/10.1186/s12974-020-02037-3
716 57 Klein, R. S. Regulation of neuroinflammation: the role of CXCL10 in lymphocyte
717 infiltration during autoimmune encephalomyelitis. *J Cell Biochem* **92**, 213-222 (2004).
718 https://doi.org/10.1002/jcb.20052

719 58 Zhong, K. *et al*. A Synthetic Steroid 5α-Androst-3β, 5, 6β-triol Alleviates Radiation-
720 Induced Brain Injury in Mice via Inhibiting GBP5/NF-κB/NLRP3 Signal Axis. *Mol*
721 *Neurobiol* **61**, 4074-4089 (2024). https://doi.org/10.1007/s12035-023-03831-9
722 59 Han, J. H. *et al*. IFITM6 expression is increased in macrophages of tumor-bearing mice.
723 *Oncol Rep* **25**, 531-536 (2011). https://doi.org/10.3892/or.2010.1092
724 60 Cunningham, C., Wilcockson, D. C., Campion, S., Lunnon, K. & Perry, V. H. Central
725 and systemic endotoxin challenges exacerbate the local inflammatory response and
726 increase neuronal death during chronic neurodegeneration. *J Neurosci* **25**, 9275-
727 9284 (2005). https://doi.org/10.1523/jneurosci.2614-05.2005
728 61 Zhao, J. *et al*. STEAP4 expression in CNS resident cells promotes Th17 cell-induced
729 autoimmune encephalomyelitis. *J Neuroinflammation* **18**, 98 (2021).
730 https://doi.org/10.1186/s12974-021-02146-7
731 62 Lester, S. N. & Li, K. Toll-like receptors in antiviral innate immunity. *J Mol Biol* **426**,
732 1246-1264 (2014). https://doi.org/10.1016/j.jmb.2013.11.024
733 63 Li, Y. *et al*. The multifaceted roles of activating transcription factor 3 (ATF3) in
734 inflammatory responses - Potential target to regulate neuroinflammation in acute
735 brain injury. *J Cereb Blood Flow Metab* **43**, 8-17 (2023).
736 https://doi.org/10.1177/0271678x231171999
737 64 Ross, J. L. *et al*. Microglia and monocyte-derived macrophages drive progression of
738 pediatric high-grade gliomas and are transcriptionally shaped by histone mutations.
739 *Immunity* **57**, 2669-2687.e2666 (2024).
740 https://doi.org/10.1016/j.immuni.2024.09.007

741 65 Krzyzowska, M., Kowalczyk, A., Skulska, K., Thörn, K. & Eriksson, K. Fas/FasL
742 Contributes to HSV-1 Brain Infection and Neuroinflammation. *Front Immunol* **12**,
743 714821 (2021). https://doi.org/10.3389/fimmu.2021.714821
744 66 Wu, S. *et al*. HSPA1A Protects Cells from Thermal Stress by Impeding ESCRT-0–
745 Mediated Autophagic Flux in Epidermal Thermoresistance. *Journal of Investigative*
746 *Dermatology* **141**, 48-58.e43 (2021).
747 https://doi.org/https://doi.org/10.1016/j.jid.2020.05.105
748 67 Kampinga, H. H. *et al*. Guidelines for the nomenclature of the human heat shock
749 proteins. *Cell Stress and Chaperones* **14**, 105-111 (2009).
750 https://doi.org/https://doi.org/10.1007/s12192-008-0068-7
751 68 Frankiw, L., Mann, M., Li, G., Joglekar, A. & Baltimore, D. Alternative splicing coupled
752 with transcript degradation modulates OAS1g antiviral activity. *Rna* **26**, 126-136
753 (2020). https://doi.org/10.1261/rna.073825.119
754 69 Bao, Z. *et al*. Prokineticin-2 prevents neuronal cell deaths in a model of traumatic
755 brain injury. *Nat Commun* **12**, 4220 (2021). https://doi.org/10.1038/s41467-021-
756 24469-y
757 70 Lei, J., Deng, Y. & Ma, S. Downregulation of TGIF2 is possibly correlated with neuronal
758 apoptosis and autism-like symptoms in mice. *Brain Behav* **12**, e2610 (2022).
759 https://doi.org/10.1002/brb3.2610
760 71 Dhossche, D. *et al*. Early-onset catatonia associated with SHANK3 mutations:
761 looking at the autism spectrum through the prism of psychomotor phenomena. *Front*
762 *Psychiatry* **14**, 1186555 (2023). https://doi.org/10.3389/fpsyt.2023.1186555

763 72 Srivastava, S. *et al*. Updated consensus guidelines on the management of Phelan-
764 McDermid syndrome. *Am J Med Genet A* **191**, 2015-2044 (2023).
765 https://doi.org/10.1002/ajmg.a.63312
766 73 Yurumez, E., Temelturk, R. D., Kaymak, B., Karabıyıkoğlu, Y. & Zengin, N. D. Catatonia
767 in autism spectrum disorders: Prevalence, functional impact, and diagnostic insights.
768 *Psychiatry Res* **342**, 116250 (2024). https://doi.org/10.1016/j.psychres.2024.116250
769 74 Monville, C., Torres, E. M. & Dunnett, S. B. Comparison of incremental and
770 accelerating protocols of the rotarod test for the assessment of motor deficits in the
771 6-OHDA model. *J Neurosci Methods* **158**, 219-223 (2006).
772 https://doi.org/10.1016/j.jneumeth.2006.06.001
773 75 Hernandez, A. R., Truckenbrod, L. M., Campos, K. T., Williams, S. A. & Burke, S. N. Sex
774 differences in age-related impairments vary across cognitive and physical
775 assessments in rats. *Behav Neurosci* **134**, 69-81 (2020).
776 https://doi.org/10.1037/bne0000352
777 76 Han, J., Fan, Y., Zhou, K., Blomgren, K. & Harris, R. A. Uncovering sex differences of
778 rodent microglia. *Journal of Neuroinflammation* **18**, 74 (2021).
779 https://doi.org/10.1186/s12974-021-02124-z
780 77 Hines, D. J., Choi, H. B., Hines, R. M., Phillips, A. G. & MacVicar, B. A. Prevention of
781 LPS-induced microglia activation, cytokine production and sickness behavior with
782 TLR4 receptor interfering peptides. *PLoS One* **8**, e60388 (2013).
783 https://doi.org/10.1371/journal.pone.0060388

784 78 Han, Q. *et al*. SHANK3 Deficiency Impairs Heat Hyperalgesia and TRPV1 Signaling in
785 Primary Sensory Neurons. *Neuron* **92**, 1279-1293 (2016).
786 https://doi.org/10.1016/j.neuron.2016.11.007
787 79 Kim, Y. E. *et al*. Endothelial SHANK3 regulates tight junctions in the neonatal mouse
788 blood-brain barrier through β-Catenin signaling. *Nat Commun* **16**, 1407 (2025).
789 https://doi.org/10.1038/s41467-025-56720-1
790 80 Atanasova, E. *et al*. Immune activation during pregnancy exacerbates ASD-related
791 alterations in Shank3-deficient mice. *Mol Autism* **14**, 1 (2023).
792 https://doi.org/10.1186/s13229-022-00532-3
793 81 Leblond, C. S. *et al*. Meta-analysis of SHANK Mutations in Autism Spectrum Disorders:
794 A Gradient of Severity in Cognitive Impairments. *PLOS Genetics* **10**, e1004580 (2014).
795 https://doi.org/10.1371/journal.pgen.1004580
796 82 Jesse, S. *et al*. Phelan McDermid Syndrome: Multiple Sclerosis as a Rare but Treatable
797 Cause for Regression-A Case Report. *Int J Mol Sci* **22** (2021).
798 https://doi.org/10.3390/ijms22052311
799 83 Faul, F., Erdfelder, E., Lang, A. G. & Buchner, A. G*Power 3: a flexible statistical power
800 analysis program for the social, behavioral, and biomedical sciences. *Behav Res*
801 *Methods* **39**, 175-191 (2007). https://doi.org/10.3758/bf03193146
802 84 Bourin, M. & Hascoët, M. The mouse light/dark box test. *European Journal of*
803 *Pharmacology* **463**, 55-65 (2003). https://doi.org/https://doi.org/10.1016/S0014-
804 2999(03)01274-3

805 85 Moy, S. S. *et al.* Mouse behavioral tasks relevant to autism: phenotypes of 10 inbred
806 strains. *Behav Brain Res* **176**, 4-20 (2007). https://doi.org/10.1016/j.bbr.2006.07.030
807 86 Kim, D., Paggi, J. M., Park, C., Bennett, C. & Salzberg, S. L. Graph-based genome
808 alignment and genotyping with HISAT2 and HISAT-genotype. *Nature Biotechnology* **37**,
809 907-915 (2019). https://doi.org/10.1038/s41587-019-0201-4
810 87 Pertea, M. *et al.* StringTie enables improved reconstruction of a transcriptome from
811 RNA-seq reads. *Nature Biotechnology* **33**, 290-295 (2015).
812 https://doi.org/10.1038/nbt.3122
813 88 Love, M. I., Huber, W. & Anders, S. Moderated estimation of fold change and
814 dispersion for RNA-seq data with DESeq2. *Genome Biol* **15**, 550 (2014).
815 https://doi.org/10.1186/s13059-014-0550-8
816 89 Goedhart, J. & Luijsterburg, M. S. VolcaNoseR is a web app for creating, exploring,
817 labeling and sharing volcano plots. *Scientific Reports* **10**, 20560 (2020).
818 https://doi.org/10.1038/s41598-020-76603-3
819 90 Heberle, H., Meirelles, G. V., da Silva, F. R., Telles, G. P. & Minghim, R. InteractiVenn: a
820 web-based tool for the analysis of sets through Venn diagrams. *BMC Bioinformatics*
821 **16**, 169 (2015). https://doi.org/10.1186/s12859-015-0611-3
822 91 Wang, S. E. *et al.* TRPV1 Regulates Stress Responses through HDAC2. *Cell Rep* **19**,
823 401-412 (2017). https://doi.org/10.1016/j.celrep.2017.03.050
824 92 Carlin, R. K., Grab, D. J., Cohen, R. S. & Siekevitz, P. Isolation and characterization of
825 postsynaptic densities from various brain regions: enrichment of different types of

826 postsynaptic densities. *J Cell Biol* **86**, 831-845 (1980).
827 https://doi.org/10.1083/jcb.86.3.831

828

829 **Figure legend:**

830 **Figure 1. LPS challenge induced selective behavioral impairments in *Sh3*$^{+/-}$ mice.**

831 **A. The body weight loss after LPS intraperitoneal injection.** Mouse was weighed
832 before injection, and at 3, 6, 24, 48, and 72 hours after LPS (1 mg/kg) or the same volume
833 of PBS injection. Each mouse's body weight was normalized to the weight before injection.
834 Two-way repeated measures ANOVA was performed (genotype/LPS effect $F_{(3, 50)} = 34.32$,
835 $p < 0.0001$; Hour effect $F_{(4, 200)} = 84.15$, $p < 0.0001$; genotype/LPS X Hour interaction F
836 $_{(12, 200)} = 22.64$, $p < 0.0001$). Post-hoc Tuckey's test showed no significant difference
837 between WT+PBS (n = 8) and *Sh3*$^{+/-}$+PBS (n = 17) or between WT+LPS (n = 8) and
838 *Sh3*$^{+/-}$+LPS (n = 21) at 3 hours, 6 hours, 24 hours, 48 hours and 72 hours after injection.
839 Mouse body weight started to reduce significantly after LPS injection compared to PBS
840 injection at 24 hours, 48 hours and 72 hours. Mouse body weight from LPS groups
841 significantly increased at 72 hours compared to 48 hours after injection in both WT+LPS
842 and *Sh3*$^{+/-}$+LPS groups. See multiple comparison statistics in Supplementary Table 5.

843 **B. Schematic drawing for the experimental design.**

844 **C-D. LPS challenge impaired motor function in *Sh3*$^{+/-}$ mice.** Steady speed rotarod (16
845 rpm, **C**) and accelerated speed rotarod (4-40 rpm, **D**) tests were performed and latency
846 to fall was measured. No significant difference was found between WT+PBS and *Sh3*$^{+/-}$
847 +PBS (16 rpm, p =0.5487, 4-40 rpm, p =0.3283) or between WT+PBS and WT+LPS (16
848 rpm, p =0.9797, 4-40 rpm, p =0.6711). *Sh3*$^{+/-}$+LPS significantly reduced latency to fall
849 compared to *Sh3*$^{+/-}$+PBS (16 rpm, p =0.0126, 4-40 rpm, p =0.0061) or compared to

850 WT+LPS (16 rpm, p =0.002, 4-40 rpm, p =0.001). *Sh3*$^{-/-}$ mice significantly reduced latency
851 to fall compared to WT+PBS (16 rpm, $p < 0.0001$, 4-40 rpm, $p < 0.0001$).

852 **E-F. LPS challenge increased anxiety-like behavior in *Sh3*$^{+/-}$ mice.** Mouse duration
853 spent in the center of the open field test and travel distance in light chamber of light/dark
854 box test were measured. No significant difference found between WT+PBS and WT+LPS
855 (OFT, p = 0.5956, light/dark box p = 0.6004). *Sh3*$^{+/-}$+LPS showed less center duration
856 than *Sh3*$^{+/-}$+PBS (p = 0.0033) despite that *Sh3*$^{+/-}$+PBS showed increased center duration
857 than WT+PBS (p = 0.0005), and *Sh3*$^{+/-}$+LPS showed less travel distance in light chamber
858 than *Sh3*$^{+/-}$+PBS (p = 0.0158) or WT+LPS (p = 0.0107).

859 **G. LPS challenge increased repetitive behavior in *Sh3*$^{+/-}$ mice.** Grooming behavior
860 was hand scored and compared. *Sh3*$^{+/-}$+LPS showed longer grooming duration than
861 *Sh3*$^{+/-}$+PBS (p = 0.0348) or WT+LPS (p = 0.0135).

862 **H-I. LPS challenge had no effect on sociability *Sh3*$^{+/-}$ mice.** Three-chamber tests were
863 conducted and duration spent in mouse chamber (S), empty chamber (E), proximity
864 regions in mouse chamber (SP) and empty chamber (EP) were compared (Two-way
865 repeated measures ANOVA. **H.** genotype effect $F_{(4, 68)} = 1.590$, p = 0.1869, S/E effect F
866 $_{(1, 68)} = 25.46$, $p < 0.0001$, genotype X S/E interaction $F_{(4, 68)} = 0.8135$, p = 0.5209; **I.**
867 genotype effect $F_{(4, 68)} = 1.398$, p = 0.2441, SP/EP effect $F_{(1, 68)} = 34$, $p < 0.0001$, genotype
868 X SP/EP interaction $F_{(4, 68)} = 0.4236$, p = 0.7911). No significant difference of duration
869 was found between S vs. E (p = 0.5325) or SP vs. EP (p = 0.2529) in *Sh3*$^{-/-}$ mice. All other
870 groups of mice showed significantly increased duration in S vs. E or SP vs. EP. * $p < 0.05$,
871 ** $p < 0.005$, *** $p < 0.0005$, **** $p < 0.0001$

872 **Figure 2. Mefenamic acid (MFA) partially improved the motor behavior deterioration**
873 **in WT and *Sh3*$^{+/-}$ mice.**

874 **A. Schematic drawing for experiment design.** Anti-inflammatory treatment with
875 intraperitoneal MFA injection was given to mice once every day for 7 days after LPS
876 injection. Rotarod tests were performed 24 hours after the last does of MFA injection.

877 **B-C. MFA partially improved the rotarod test performance.** After 1-week treatment of
878 MFA, Steady speed rotarod (16 rpm, **B**) and accelerated speed rotarod (4-40 rpm, **C**)
879 tests were performed and latency to fall was compared. (Two-way ANOVA, **B. 16 rpm,**
880 LPS/MFA effect $F_{(1, 37)} = 23.66$, $p < 0.0001$, genotype effect $F_{(1,46)} = 1.859$, $p = 0.1794$,
881 LPS/MFA X genotype interaction $F_{(1, 37)} = 0.8697$, $p = 0.3571$. **C. 4-40 rpm,** LPS/MFA
882 effect $F_{(1, 85)} = 1.721$, $p = 0.1932$, genotype effect $F_{(1,85)} = 4.822$, $p = 0.0308$, LPS/MFA X
883 genotype interaction $F_{(1, 85)} = 0.8220$, $p = 0.3672$). Compared to vehicle group, MFA-
884 treated *Sh3*$^{+/-}$ and WT mice showed increased latency to fall in 16 rpm rotarod test (*Sh3*$^{+/-}$,
885 $p = 0.0091$; WT, $p = 0.0002$).

886 **D-E. MFA treatment was more effective in female *Sh3*$^{+/-}$ mice than male ones.** Two-
887 way ANOVA was performed to compare sex difference in MFA treatment (**D. 16 rpm,**
888 LPS/MFA effect $F_{(1, 43)} = 4.626$, $p = 0.0372$, sex effect $F_{(1,43)} = 9.227$, $p = 0.004$, LPS/MFA
889 X sex interaction $F_{(1, 43)} = 1.858$, $p = 0.1799$. **E. 4-40 rpm,** LPS/MFA effect $F_{(1, 16)} = 2.065$,
890 $p = 0.17$, sex effect $F_{(1,29)} = 2.369$, $p = 0.1346$, LPS/MFA X sex interaction $F_{(1, 16)} = 8.046$,
891 $p = 0.0119$). MFA-treated female *Sh3*$^{+/-}$ showed significantly higher latency to fall
892 compared to vehicle-treated female *Sh3*$^{+/-}$ (16 rpm, $p = 0.0229$; 40rpm, $p = 0.0106$) and
893 MFA-treated male *Sh3*$^{+/-}$ (16 rpm, $p = 0.0009$; 40rpm, $p = 0.0011$). * $p < 0.05$, ** $p < 0.005$,
894 *** $p < 0.0005$, **** $p < 0.0001$

895 **Figure 3. Bulk RNA sequencing revealed distinct molecular mechanism underlying**
896 **LPS effect on *Sh3*$^{+/-}$ mice.**

897 **A-D. The volcano plot shows differentially expressed genes (DEGs) distribution.**
898 DEGs were identified in four comparisons: *Sh3*$^{+/-}$+LPS vs *Sh3*$^{+/-}$+PBS (**A**), WT+LPS vs.
899 WT+PBS (**B**), *Sh3*$^{+/-}$+LPS vs. WT+LPS (**C**), *Sh3*$^{+/-}$+PBS vs. WT+PBS (**D**). Upregulated
900 genes are indicated in red color, downregulated genes are indicated in blue color and
901 DEGs below threshold are indicated in grey color.

902 **E-F. Venn diagrams show shared upregulated and downregulated genes among**
903 **four comparisons.** Shared upregulated (**E**) and downregulated genes (**F**) numbers are
904 shown within the diagrams. Comparison of *Sh3*$^{+/-}$+LPS vs *Sh3*$^{+/-}$+PBS is red diagram,
905 WT+LPS vs. WT+PBS is blue diagram, *Sh3*$^{+/-}$+LPS vs. WT+LPS is green diagram, and
906 *Sh3*$^{+/-}$+PBS vs. WT+PBS is yellow diagram.

907 **G. Bubble chart shows functions of DEGs of *Sh3*$^{+/-}$+LPS vs. WT+LPS comparison.**
908 Volcano plot of the negative log of p-value (Y-axis) vs. the z-score (X-axis). *p*-value was
909 calculated using the right-tailed Fisher's Exact Test. A negative log of p-value cutoff of
910 1.3 ($p < 0.05$) was used to identify significantly changed functional pathways. A z-score
911 range cutoff of ±0.1 was used to identify the activation or inhibition state of a canonical
912 pathway. Some names of pathways are annotated in the chart. Activated pathways are
913 orange bubbles and inhibited pathways are blue bubbles. The size of the bubbles reflects
914 the number of genes overlapped with the pathway database.

915 **Figure 4. Neuroinflammation increased in *Sh3*$^{+/-}$ mice compared to WT mice in**
916 **response to LPS.**

917 **A-D. Differential expression of neuroinflammatory marker genes *Il1b*, *Cxcl10,***
918 ***Cx3cr1* and *P2ry12*.** At 24 hours after LPS injection, forebrain RNA was extracted, and
919 RT-qPCR was performed. Target gene expression was normalized to the expression of
920 the housekeeping gene GAPDH. One-way ANOVA was performed to compare gene
921 expression in four groups (*Il1b*: F= 14.93, p = 0.0004, *Cxcl10*: F= 16.73, p = 0.0002,
922 *Cx3cr1*: F= 14.8, p < 0.0001, *P2ry12*: F= 8.442, p = 0.0002). As expected, compared to
923 PBS treatment, LPS significantly increased expression of *Il1b, Cxcl10*, and *Cx3cr1*, and
924 decreased expression of *P2ry12* in both WT and *Sh3*$^{+/-}$ mice (WT+PBS vs. WT+LPS, *Il1b*:
925 p = 0.0005, *Cxcl10*: p = 0.0105, *Cx3cr1*: p = 0.0388, *P2ry12*: p = 0.0241; *Sh3*$^{+/-}$ +PBS vs.
926 *Sh3*$^{+/-}$ +LPS, *Il1b*: p = 0.002, *Cxcl10*: p = 0.0015, *Cx3cr1*: p < 0.0001, *P2ry12*: p = 0.0046).
927 Significant increase of *Il1b, Cxcl10*, *Cx3cr1* was observed in *Sh3*$^{+/-}$+LPS vs. WT+LPS
928 (*Il1b*: p = 0.0166, *Cxcl10*: p = 0.0076, *Cx3cr1*: p = 0.0004). In contrast, significantly
929 increased expression of *P2ry12* was observed in *Sh3*$^{+/-}$+PBS vs. WT+PBS (p = 0.0102)
930 and *Sh3*$^{+/-}$+LPS vs. WT+LPS (p = 0.036).

931 **E-H. Increased immunohistochemistry fluorescence intensity of IBA1 in *Sh3*$^{+/-}$**
932 **+LPS mice.** Mouse brain slices were collected at 3 hours and 24 hours after injection,
933 respectively. Microglia activation was labeled with IBA1 antibody. Quantitative
934 fluorescence intensity of IBA1 at cortex regions from WT+LPS, *Sh3*$^{+/-}$+PBS, and *Sh3*$^{+/-}$
935 +LPS were normalized to WT+PBS group and then compared (Kruskal-Wallis test, **G.** p
936 = 0.0002; **H.** p < 0.0001). LPS increased microglia activation in both WT and *Sh3*$^{+/-}$ mice
937 at both 3 hours and 24 hours after injection compared to PBS groups (WT+PBS vs.

938 WT+LPS, 3 hours, p = 0.0067, 24 hours, p = 0.0053; *Sh3*$^{+/-}$ +PBS vs. *Sh3*$^{+/-}$ +LPS, 3
939 hours, p = 0.0004, 24 hours, p < 0.0001). Moreover, LPS induced significant
940 overactivation of microglia in *Sh3*$^{+/-}$ mice at 24 hours after injection compared to WT mice,
941 not 3 hours (WT+LPS vs. *Sh3*$^{+/-}$ +LPS, 3 hours, p = 0.6204, 24 hours, p = 0.0017). * p <
942 0.05, ** p < 0.005, *** p < 0.0005, **** p < 0.0001.

943 **Figure 5. Elevated TLR4 expression and reduced HOMER 1b/c and PSD95**
944 **expression in *Sh3*$^{+/-}$ mice.**

945 **A-D. Increased TLR4 and decreased SHANK3 protein expression in S*h3*$^{+/-}$ mice.** LPS
946 receptor TLR4 (**A-B**) and SHANK3 (**C-D**) expression were examined in whole-cell lysates
947 using western blot at 24 hours after injection. Target protein expression was normalized
948 to β-ACTIN expression. Quantitative protein expression from WT+LPS, *Sh3*$^{+/-}$+PBS, and
949 *Sh3*$^{+/-}$+LPS were normalized to WT+PBS group and then compared. Significantly
950 elevated TLR4 expression was observed in *Sh3*$^{+/-}$ mice compared to WT mice (WT+PBS
951 vs. *Sh3*$^{+/-}$ +PBS, $p < 0.0001$; WT+LPS vs. *Sh3*$^{+/-}$ +LPS, $p = 0.0081$). As expected,
952 significantly reduced SHANK3 expression was detected in *Sh3*$^{+/-}$ mice (WT+PBS vs.
953 *Sh3*$^{+/-}$ +PBS, $p = 0.0172$; WT+LPS vs. *Sh3*$^{+/-}$ +LPS, $p = 0.002$).

954 **E-J. Colocalization analysis of TLR4/IBA1 between WT+LPS vs. *Sh3*$^{+/-}$ +LPS.** No
955 difference in colocalization Pearson's coefficient between WT+LPS vs. *Sh3*$^{+/-}$ +LPS was
956 observed ($p = 0.2309$). *Sh3*$^{+/-}$ showed smaller normalized colocalization by TLR4 ($p =$
957 0.0093) but similar normalized colocalization by IBA1 ($p = 0.9141$) compared to WT. *Sh3*$^{+/-}$
958 showed decreased TLR4 cellular fluorescence intensity ($p = 0.0183$) but increased IBA1
959 cellular fluorescence intensity ($p = 0.0001$) than WT.

960 **L-N. Reduced postsynaptic density (PSD) protein HOMER 1b/c and PSD95**
961 **expression in *Sh3*$^{+/-}$ mice.** HOMER 1b/c and PSD95 expression were examined in PSD
962 fraction of forebrain using western blot at 2 weeks after injection. Target protein
963 expression was normalized to β-ACTIN expression. Quantitative protein expression from
964 WT+LPS, *Sh3*$^{+/-}$+PBS, and *Sh3*$^{+/-}$+LPS were normalized to WT+PBS group and then
965 compared. Significantly reduced HOMER 1b/c expression was observed in *Sh3*$^{+/-}$ mice

966 (WT+PBS vs. *Sh3*$^{+/-}$ +PBS, $p < 0.0001$; WT+LPS vs. *Sh3*$^{+/-}$+LPS, $p = 0.0088$). Significant

967 decreased PSD95 expression was detected in *Sh3*$^{+/-}$+LPS compared to WT+LPS group

968 ($p = 0.0007$). * $p < 0.05$, ** $p < 0.005$, *** $p < 0.0005$, **** $p < 0.0001$.

969

970 **Figure 6. Summary of increased neuroinflammation susceptibility in *Sh3*$^{+/-}$ mice.**

Figure 1

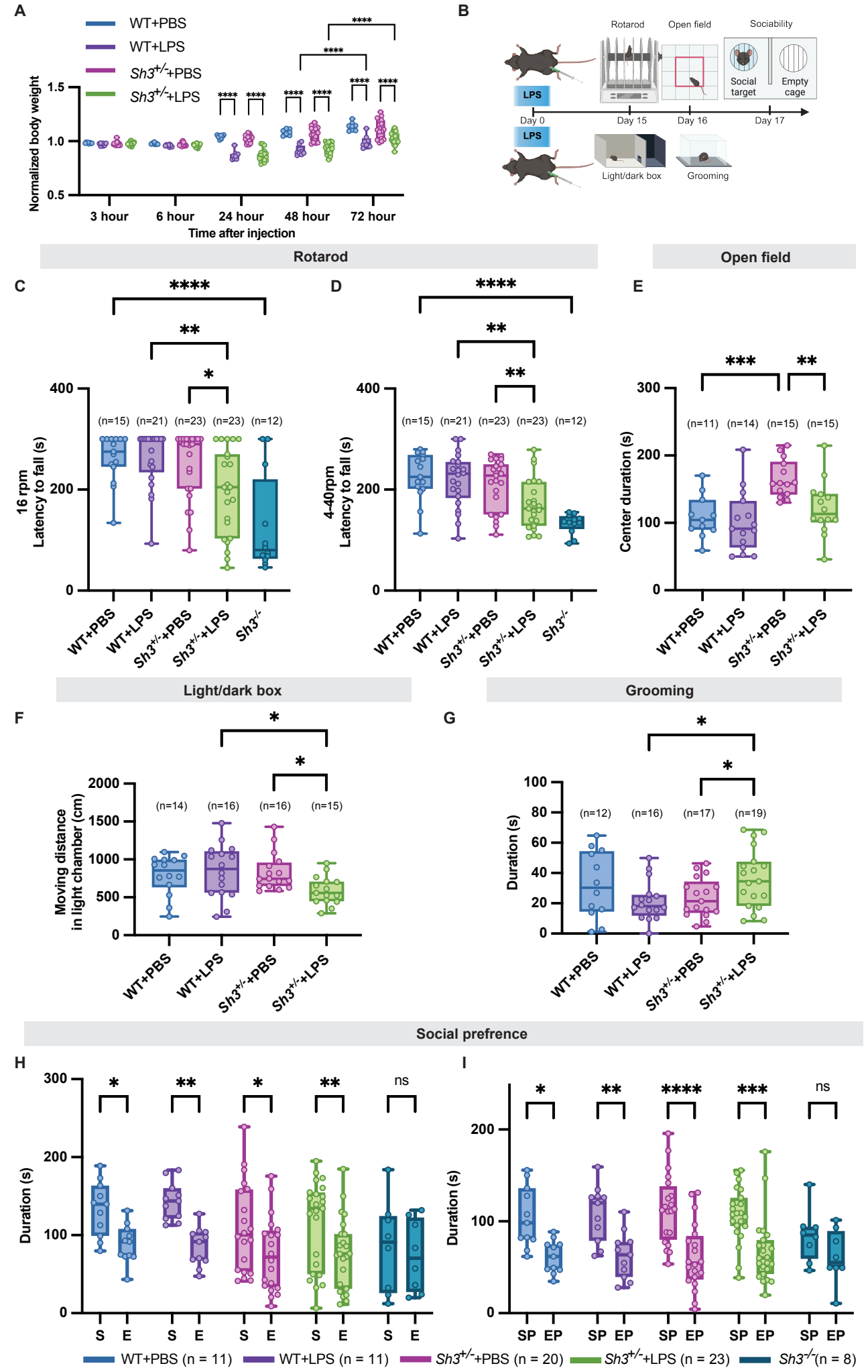
A
WT+PBS
WT+LPS
Sh3+/-+PBS
Sh3+/-+LPS
Normalized body weight
1.5
1.0
0.5
3 hour
6 hour
24 hour
48 hour
72 hour
Time after injection
B
Rotarod
Open field
Sociability
Social target
Empty cage
LPS
Day 0
Day 15
Day 16
Day 17
Light/dark box
Grooming
Rotarod
Open field
C
16 rpm Latency to fall (s)
(n=15) (n=21) (n=23) (n=23) (n=12)
D
4-40rpm Latency to fall (s)
(n=15) (n=21) (n=23) (n=23) (n=12)
E
Center duration (s)
(n=11) (n=14) (n=15) (n=15)
WT+PBS
WT+LPS
Sh3+/-+PBS
Sh3+/-+LPS
Sh3-/-
Light/dark box
Grooming
F
Moving distance in light chamber (cm)
(n=14) (n=16) (n=16) (n=15)
G
Duration (s)
(n=12) (n=16) (n=17) (n=19)
Social prefrence
H
Duration (s)
S E S E S E S E S E
I
Duration (s)
SP EP SP EP SP EP SP EP SP EP
WT+PBS (n = 11)
WT+LPS (n = 11)
Sh3+/-+PBS (n = 20)
Sh3+/-+LPS (n = 23)
Sh3-/-(n = 8)

Figure 2

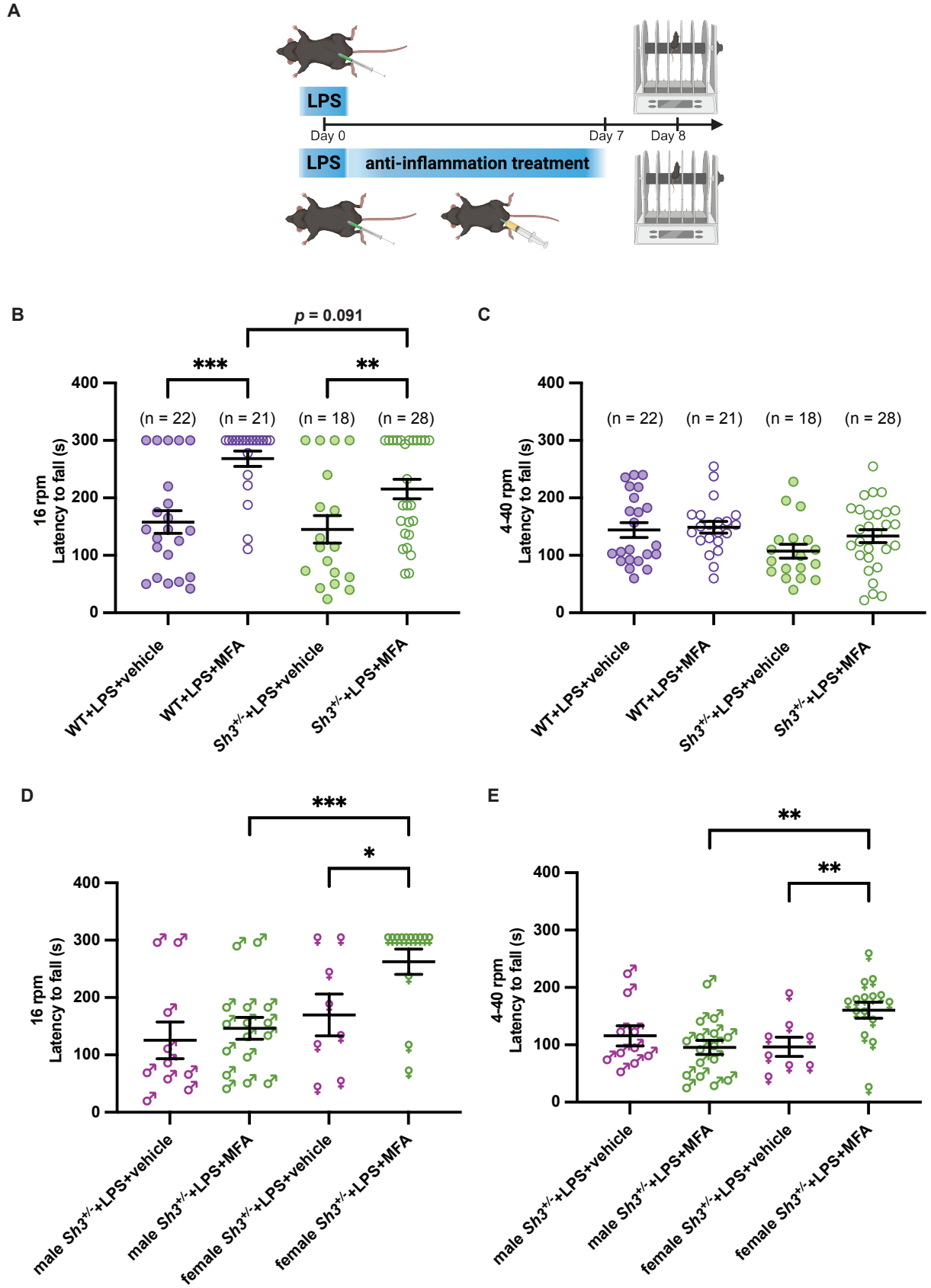
A
LPS
Day 0
Day 7
Day 8
LPS
anti-inflammation treatment
B
p = 0.091
***
**
(n = 22)
(n = 21)
(n = 18)
(n = 28)
16 rpm
Latency to fall (s)
400
300
200
100
0
WT+LPS+vehicle
WT+LPS+MFA
Sh3+/-+LPS+vehicle
Sh3+/-+LPS+MFA
C
(n = 22)
(n = 21)
(n = 18)
(n = 28)
4-40 rpm
Latency to fall (s)
400
300
200
100
0
WT+LPS+vehicle
WT+LPS+MFA
Sh3+/-+LPS+vehicle
Sh3+/-+LPS+MFA
D
***
*
16 rpm
Latency to fall (s)
400
300
200
100
0
male Sh3+/-+LPS+vehicle
male Sh3+/-+LPS+MFA
female Sh3+/-+LPS+vehicle
female Sh3+/-+LPS+MFA
E
**
**
4-40 rpm
Latency to fall (s)
400
300
200
100
0
male Sh3+/-+LPS+vehicle
male Sh3+/-+LPS+MFA
female Sh3+/-+LPS+vehicle
female Sh3+/-+LPS+MFA

Figure 3

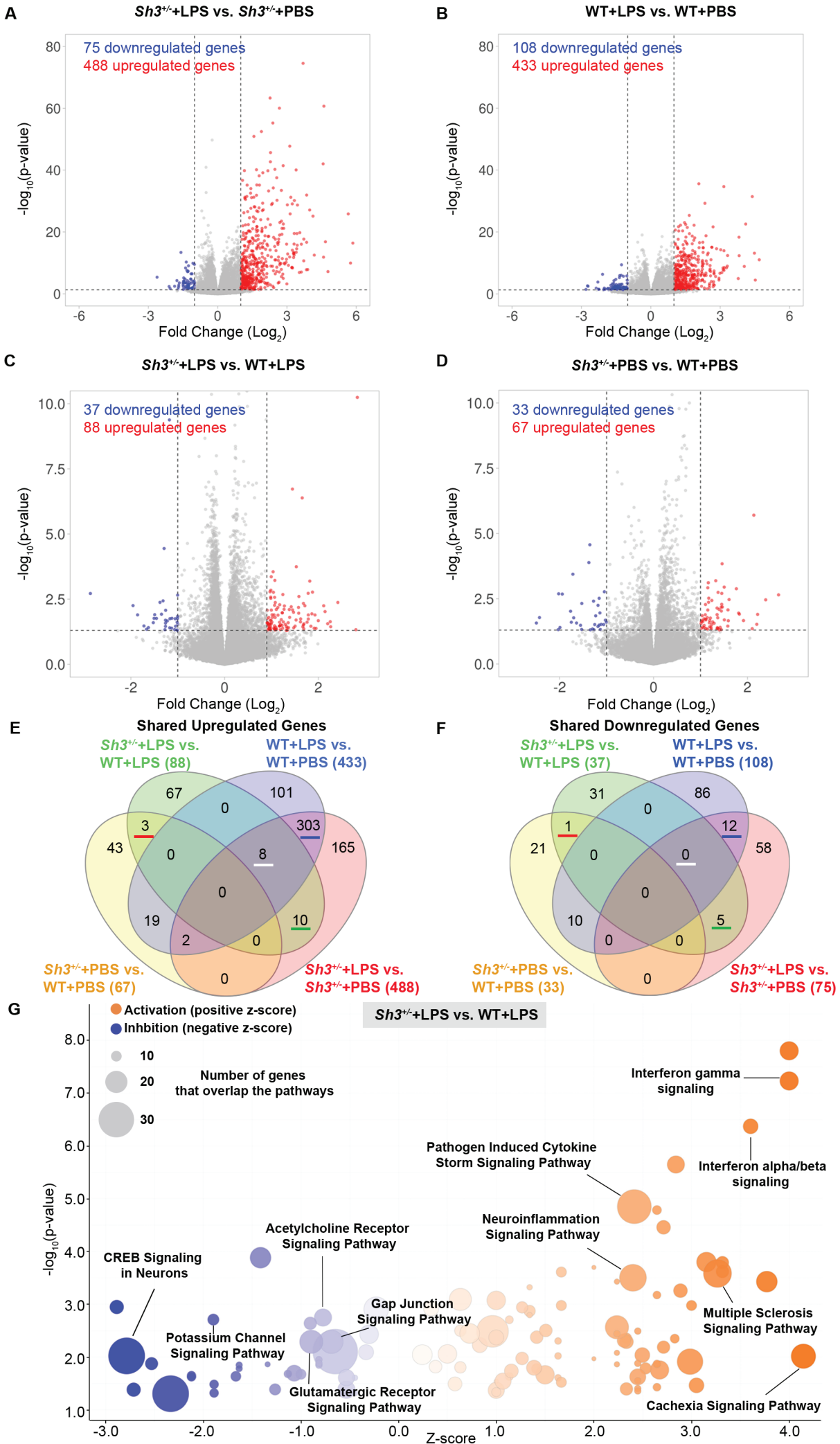
A
Sh3+/-+LPS vs. Sh3+/-+PBS
75 downregulated genes
488 upregulated genes
-log10(p-value)
Fold Change (Log2)
B
WT+LPS vs. WT+PBS
108 downregulated genes
433 upregulated genes
C
Sh3+/-+LPS vs. WT+LPS
37 downregulated genes
88 upregulated genes
D
Sh3+/-+PBS vs. WT+PBS
33 downregulated genes
67 upregulated genes
E
Shared Upregulated Genes
Sh3+/-+LPS vs. WT+LPS (88)
WT+LPS vs. WT+PBS (433)
Sh3+/-+PBS vs. WT+PBS (67)
Sh3+/-+LPS vs. Sh3+/-+PBS (488)
F
Shared Downregulated Genes
Sh3+/-+LPS vs. WT+LPS (37)
WT+LPS vs. WT+PBS (108)
Sh3+/-+PBS vs. WT+PBS (33)
Sh3+/-+LPS vs. Sh3+/-+PBS (75)
G
Sh3+/-+LPS vs. WT+LPS
Activation (positive z-score)
Inhbition (negative z-score)
Number of genes that overlap the pathways
Interferon gamma signaling
Interferon alpha/beta signaling
Pathogen Induced Cytokine Storm Signaling Pathway
Neuroinflammation Signaling Pathway
Acetylcholine Receptor Signaling Pathway
CREB Signaling in Neurons
Gap Junction Signaling Pathway
Multiple Sclerosis Signaling Pathway
Potassium Channel Signaling Pathway
Glutamatergic Receptor Signaling Pathway
Cachexia Signaling Pathway
Z-score

Figure 4

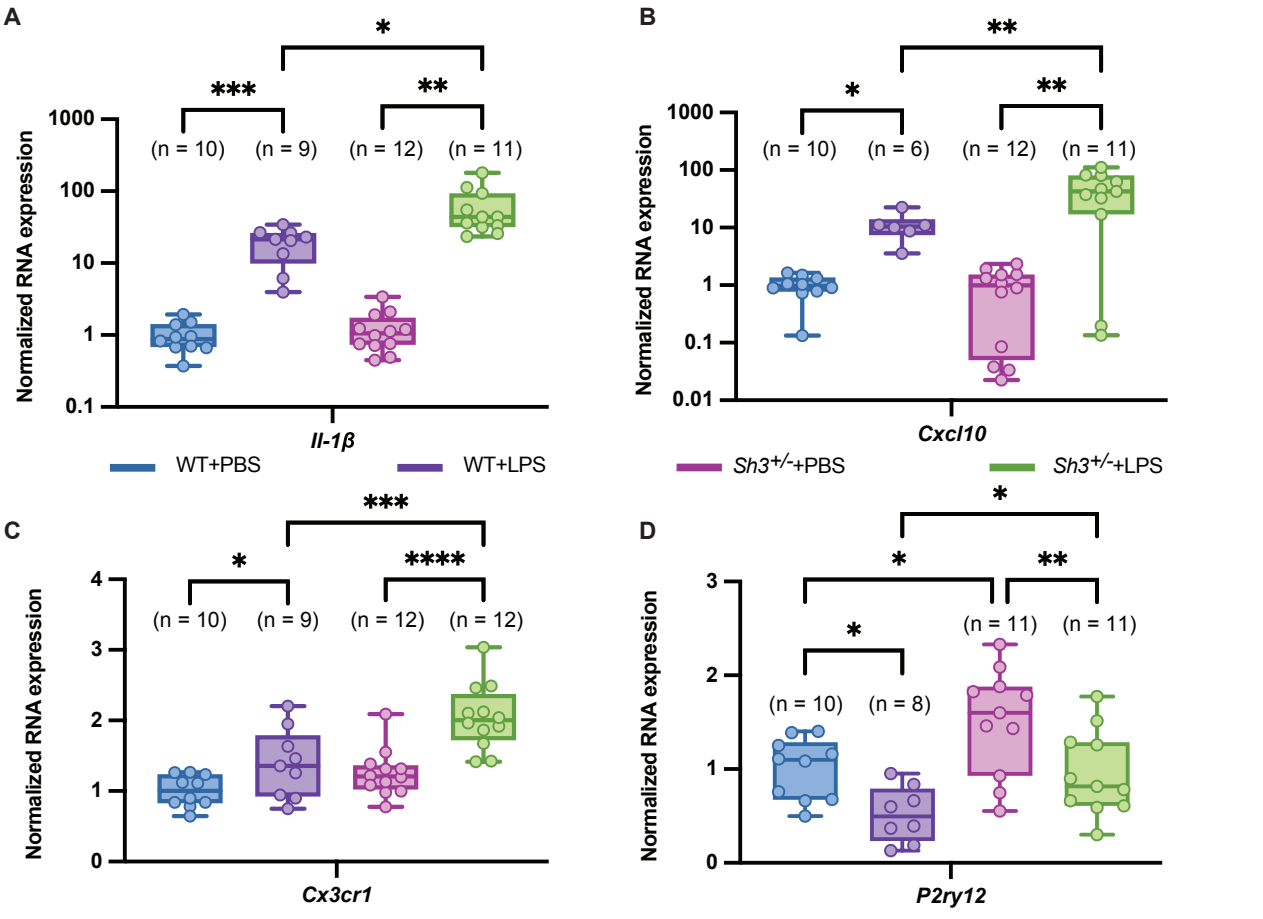
A
B
C
D
Normalized RNA expression
Il-1β
Cxcl10
Cx3cr1
P2ry12
(n = 10)
(n = 9)
(n = 12)
(n = 11)
(n = 6)
(n = 8)
WT+PBS
WT+LPS
Sh3+/-+PBS
Sh3+/-+LPS

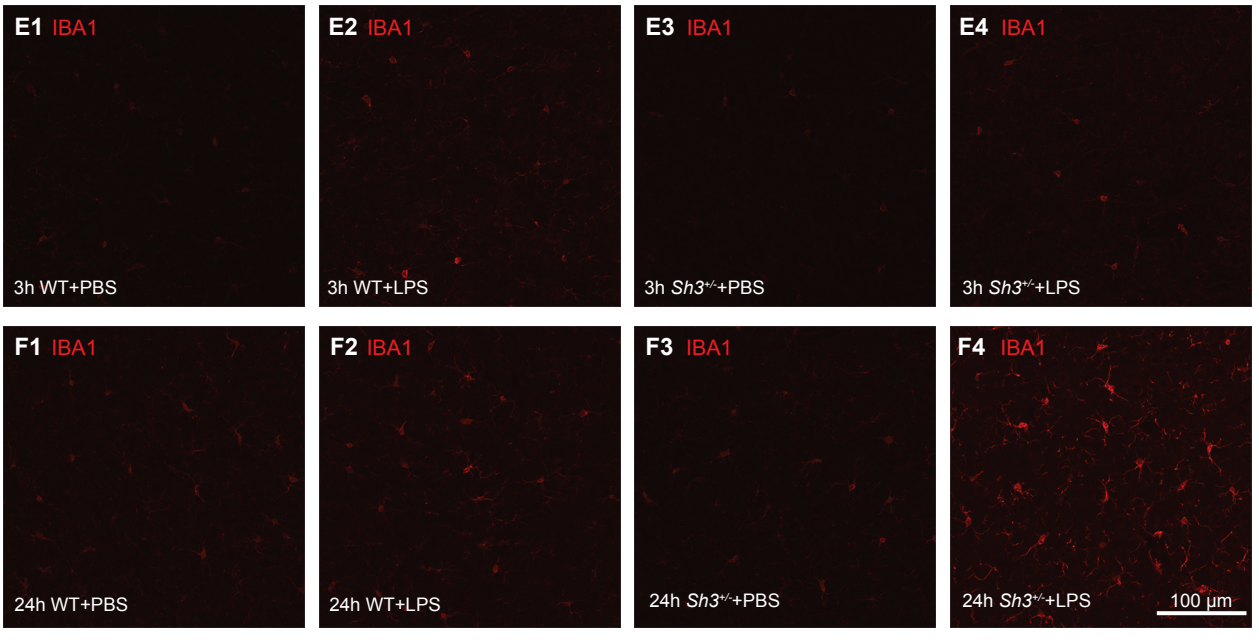
E1 IBA1
3h WT+PBS
E2 IBA1
3h WT+LPS
E3 IBA1
3h Sh3+/-+PBS
E4 IBA1
3h Sh3+/-+LPS
F1 IBA1
24h WT+PBS
F2 IBA1
24h WT+LPS
F3 IBA1
24h Sh3+/-+PBS
F4 IBA1
24h Sh3+/-+LPS
100 µm

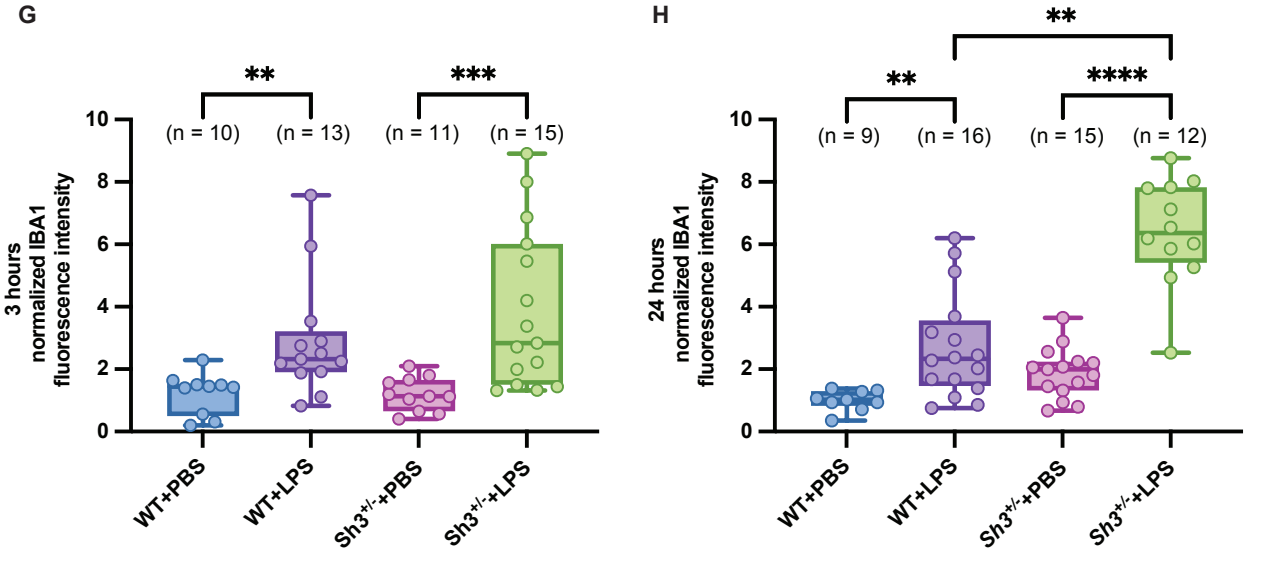
G
H
3 hours normalized IBA1 fluorescence intensity
24 hours normalized IBA1 fluorescence intensity
(n = 10)
(n = 13)
(n = 11)
(n = 15)
(n = 9)
(n = 16)
(n = 15)
(n = 12)
WT+PBS
WT+LPS
Sh3+/-+PBS
Sh3+/-+LPS

Figure 5

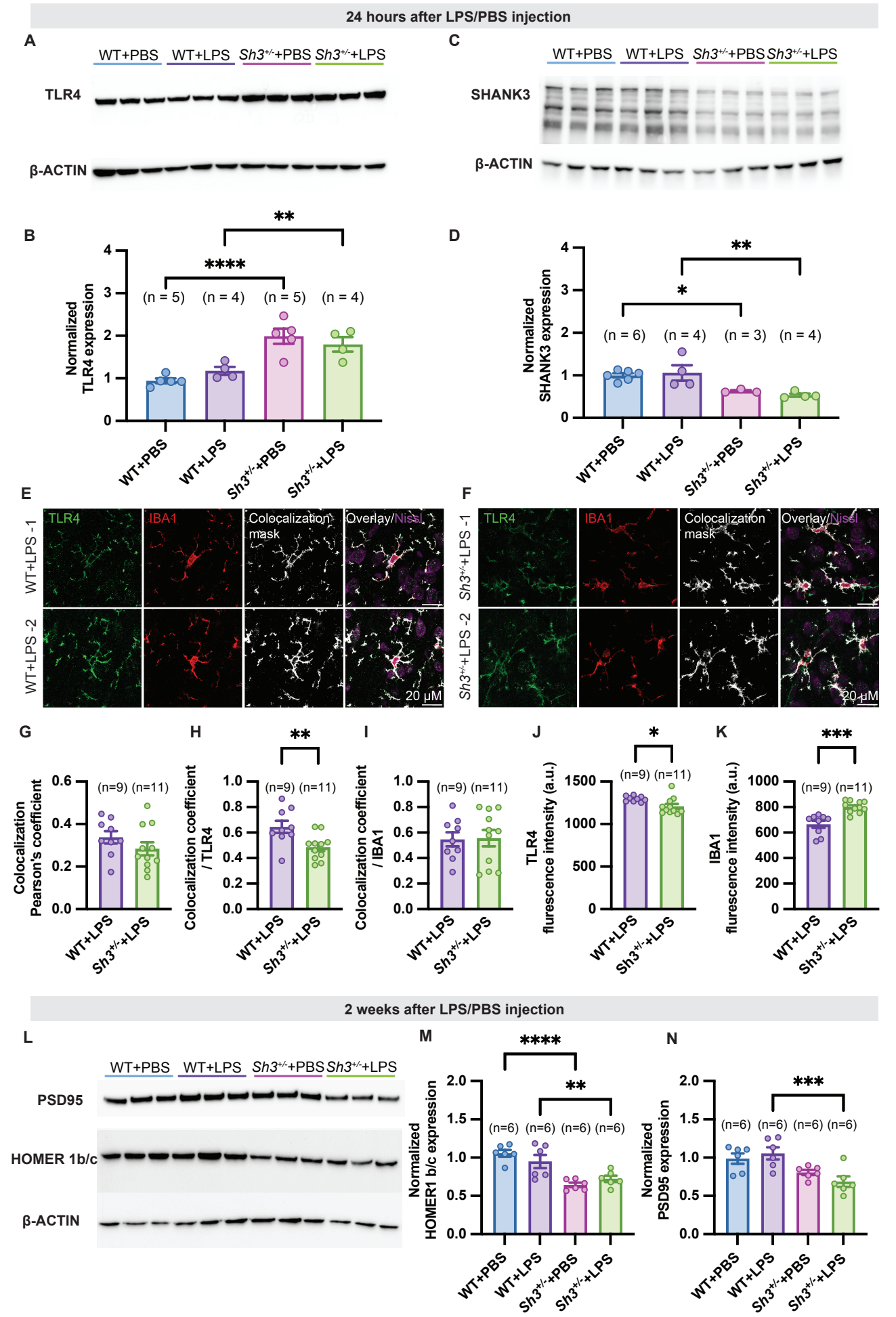
24 hours after LPS/PBS injection
A
WT+PBS
WT+LPS
Sh3+/-+PBS
Sh3+/-+LPS
TLR4
β-ACTIN
B
Normalized TLR4 expression
(n = 5)
(n = 4)
(n = 5)
(n = 4)
****
**
C
SHANK3
β-ACTIN
D
Normalized SHANK3 expression
(n = 6)
(n = 4)
(n = 3)
(n = 4)
*
**
E
WT+LPS -1
WT+LPS -2
TLR4
IBA1
Colocalization mask
Overlay/Nissl
20 μM
F
Sh3+/-+LPS -1
Sh3+/-+LPS -2
G
Colocalization Pearson's coefficient
(n=9) (n=11)
H
Colocalization coefficient / TLR4
I
Colocalization coefficient / IBA1
J
TLR4 fluorescence intensity (a.u.)
*
K
IBA1 fluorescence intensity (a.u.)
***
WT+LPS
Sh3+/-+LPS
2 weeks after LPS/PBS injection
L
PSD95
HOMER 1b/c
β-ACTIN
M
Normalized HOMER1 b/c expression
(n=6)
****
**
N
Normalized PSD95 expression
***

Figure 6

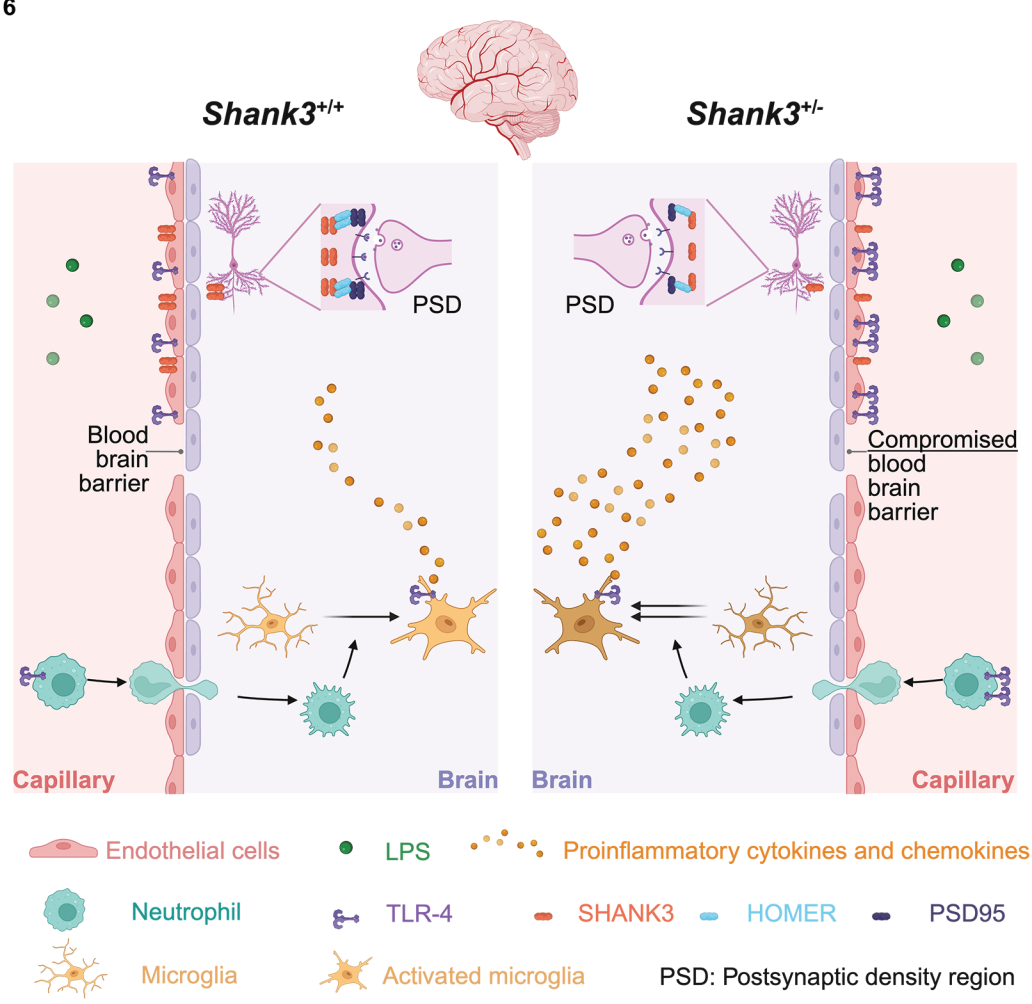
Shank3+/+
Shank3+/-
PSD
PSD
Blood brain barrier
Compromised blood brain barrier
Capillary
Brain
Brain
Capillary
Endothelial cells
LPS
Proinflammatory cytokines and chemokines
Neutrophil
TLR-4
SHANK3
HOMER
PSD95
Microglia
Activated microglia
PSD: Postsynaptic density region